

Explaining Explainability: Understanding Concept Activation Vectors

Angus Nicolson^{1,2}, Lisa Schut², J. Alison Noble¹, and Yarin Gal²

¹ Institute of Biomedical Engineering, University of Oxford
angus.nicolson@eng.ox.ac.uk

² OATML, Department of Computer Science, University of Oxford

Abstract. Recent interpretability methods propose using concept-based explanations to translate the internal representations of deep learning models into a language that humans are familiar with: concepts. This requires understanding which concepts are present in the representation space of a neural network. One popular method for finding concepts is Concept Activation Vectors (CAVs), which are learnt using a probe dataset of concept exemplars. In this work, we investigate three properties of CAVs. CAVs may be: (1) inconsistent between layers, (2) entangled with different concepts, and (3) spatially dependent. Each property provides both challenges and opportunities in interpreting models. We introduce tools designed to detect the presence of these properties, provide insight into how they affect the derived explanations, and provide recommendations to minimise their impact. Understanding these properties can be used to our advantage. For example, we introduce spatially dependent CAVs to test if a model is translation invariant with respect to a specific concept and class. Our experiments are performed on ImageNet and a new synthetic dataset, Elements. Elements is designed to capture a known ground truth relationship between concepts and classes. We release this dataset to facilitate further research in understanding and evaluating interpretability methods.

Keywords: Interpretability · Explainable AI · Concepts

1 Introduction

Deep learning models have become ubiquitous, achieving performance reaching or surpassing human experts across a variety of tasks. However, currently, the inherent complexity of these models obfuscates our ability to explain their decision-making process. As they are applied in a growing number of real-world domains, there is an increasing need to understand how they work. This transparency allows for easier debugging and better understanding of model limitations.

Model explanations can take many forms, such as input features, prototypes or concepts. Recent work has shown that explainability methods that focus on low-level features can incur problems. For example, saliency methods can suffer from confirmation bias and lack faithfulness [2]. Even when faithful, they only show ‘where’ the model focused in the image, and not ‘what’ it focused on [1, 9].

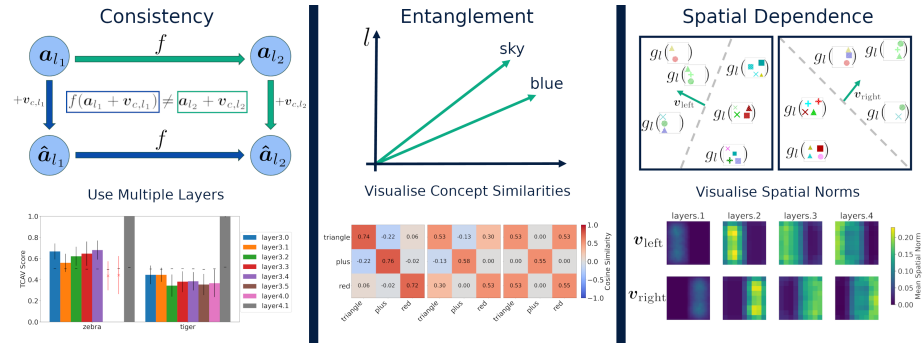


Fig. 1: Concept Activation Vectors can be: inconsistent, i.e., we cannot find two concept vectors in different layers that have the same additive effect (left), entangled (middle) and spatially dependent (right). The top panel illustrates each of these different properties. The bottom panels show our recommendations on how to minimise the impact these effects can have: creating CAVs for multiple layers (left), verifying expected dependencies between related concepts (middle), and visualising spatial dependence (right).

To address these problems, concept-based methods provide explanations using high-level terms that humans are familiar with. A popular method is concept activation vectors (CAVs): a linear representation of a concept found in the activation space of a specific layer using a probe dataset of concept examples [23]. However, concept-based methods also face challenges, such as their sensitivity to the specific probe dataset [34, 38].

In this paper, we focus on understanding three properties of concept vectors:

1. They cannot be **consistent** across layers,
2. They can be **entangled** with other concepts,
3. They can be **spatially dependent**.

We provide tools to analyse each property and show that they can affect testing with CAVs (TCAV) (§6.1, §6.2 and §6.3). To minimise the impact these effects can have, we recommend: creating CAVs for multiple layers, verifying expected dependencies between related concepts, and visualising spatial dependence (§7). These properties do not imply that CAVs should not be used. On the contrary, we may be able to use these properties to better understand model behaviour. For example, we introduce a modified version of CAVs that are spatially dependent and can be used to identify translation invariance in convolutional neural networks (CNNs).

To help explore these properties, we created a configurable synthetic dataset: Elements (§4). This dataset provides control over the ground-truth relationships between concepts and classes in order to understand model behaviour. Using the Elements dataset, researchers can study (1) the faithfulness of a concept-based explanation method and (2) the concept entanglement in a network.

2 Background: Concept Activation Vectors

A CAV [23] is a vector representation of a concept found in the activation space of a layer of a NN. Consider a NN which can be decomposed into two functions: $g_l(\mathbf{x}) = \mathbf{a}_l \in \mathbb{R}^m$ which maps the input $\mathbf{x} \in \mathbb{R}^n$ to a vector \mathbf{a}_l in the activation space of layer l , and $h_l(\mathbf{a}_l)$ which maps \mathbf{a}_l to the output. To create a CAV for a concept c we need a probe dataset \mathbb{D}_c consisting of positive samples \mathbb{X}_c^+ (concept examples), and negative samples \mathbb{X}_c^- (random in-distribution images). For the sets \mathbb{X}_c^- and \mathbb{X}_c^+ , we create a corresponding set of activations in layer l :

$$\mathbb{A}_{c,l}^+ = \{g_l(\mathbf{x}_i) \mid \forall \mathbf{x}_i \in \mathbb{X}_c^+\}, \text{ and } \mathbb{A}_{c,l}^- = \{g_l(\mathbf{x}_i) \mid \forall \mathbf{x}_i \in \mathbb{X}_c^-\}, \quad (1)$$

We find the CAV $\mathbf{v}_{c,l}$ by training a binary linear classifier to distinguish between the sets $\mathbb{A}_{c,l}^+$ and $\mathbb{A}_{c,l}^-$:

$$\mathbf{a}_l \cdot \mathbf{v}_{c,l} + b_{c,l} > 0 \quad \forall \mathbf{a}_l \in \mathbb{A}_{c,l}^+, \text{ and } \mathbf{a}_l \cdot \mathbf{v}_{c,l} + b_{c,l} \leq 0 \quad \forall \mathbf{a}_l \in \mathbb{A}_{c,l}^-, \quad (2)$$

where $\mathbf{v}_{c,l}$ is the normal vector of the hyperplane separating the activations $\mathbb{A}_{c,l}^+$ and $\mathbb{A}_{c,l}^-$, and $b_{c,l}$ is the intercept.³

To analyse a model’s sensitivity to $\mathbf{v}_{c,l}$, Kim *et al.* [23] introduce testing with CAVs (TCAV), which determines the model’s conceptual sensitivity across an entire class. Let \mathbb{X}_k be a set of inputs belonging to class k . The TCAV score is defined as

$$\text{TCAV}_{c,k,l} = \frac{|\{\mathbf{x} \in \mathbb{X}_k : S_{c,k,l}(\mathbf{x}) > 0\}|}{|\mathbb{X}_k|}, \quad (3)$$

where the directional derivative of the concept, $S_{c,k,l}$, defined as

$$S_{c,k,l}(\mathbf{x}) = \lim_{\epsilon \rightarrow 0} \frac{h_{l,k}(g_l(\mathbf{x}) + \epsilon \mathbf{v}_{c,l}) - h_{l,k}(g_l(\mathbf{x}))}{\epsilon} = \nabla h_{l,k}(g_l(\mathbf{x})) \cdot \mathbf{v}_{c,l} \quad (4)$$

where $\nabla h_{l,k}$ is the partial derivative of the NN output for class k to the activation. The TCAV score measures the fraction of class k inputs whose activation at layer l is positively influenced by concept c . A statistical test comparing the scores of CAVs to random vectors is used to determine the concept’s significance (see Appendix 11.1).

3 CAV Hypotheses

To use CAV-based explanation methods in practice, it is important to understand how they work. Therefore, we study three properties of CAVs and their effects on TCAV scores. We focus on these hypotheses as they provide insight into network representations and into the meaning encoded by concept vectors.

We formalise each property through a null hypothesis, which we provide evidence to reject later in the paper. In the following text, we use the typesetting **concept** to denote a concept.

³ Eq. 2 assumes that the linear classifier has hard boundaries. In practice, the classifiers typically achieve 80-95% accuracy.

3.1 Consistency

In general, we want to understand *model* behaviour. However, CAVs explain whether a model is sensitive to a concept in a specific *layer*. In practice, analysing all layers may be computationally infeasible, and it is unclear which layers to choose. Therefore, our first hypothesis explores the relationship between CAVs found in different layers. Recall that the TCAV scores depend on the directional derivative: *how the model output changes for an infinitesimal change of the activations in the direction of a CAV*. By perturbing the activations in the direction of a CAV, we explore whether two concept vectors found in different layers can have the same affect on the model output. We refer to this property as *consistency* (see Figure 1 for a schematic overview).

Definition 1 (consistent). *Assume we have a function $f(\cdot)$ that maps the activations from layer l_1 into activations in layer l_2 , where $l_1 < l_2$. Concept vectors, \mathbf{v}_{c,l_1} and \mathbf{v}_{c,l_2} are consistent iff for every input \mathbf{x} and corresponding activations \mathbf{a}_{l_1} and \mathbf{a}_{l_2} , $f(\mathbf{a}_{l_1} + \mathbf{v}_{c,l_1}) = \mathbf{a}_{l_2} + \mathbf{v}_{c,l_2}$.*

If two CAVs are consistent then they have the same downstream affect on the model when activations are perturbed in their direction, *i.e.*, even though they are in different layers, they have an equivalent effect on the model output and therefore the model assigns them the same meaning. Our first hypothesis is:

Null Hypothesis 1 (NH1): *Concept vector representations are consistent across layers*

In §6.1 we formally explore this hypothesis, and perform empirical evaluations on the Elements and ImageNet [12] datasets. We show theoretically the conditions \mathbf{v}_{c,l_2} and \mathbf{a}_{l_1} must meet for vectors \mathbf{v}_{c,l_1} and \mathbf{v}_{c,l_2} to be consistent when f is either a rectified linear unit (ReLU) or sigmoid function.

3.2 Entangled concept vectors

Consider the meaning encoded by a concept vector. We label a CAV using the corresponding label of the probe dataset. For example, a CAV may be labelled **striped** or **red**. This implicitly assumes that the label is a complete and accurate description of the information encoded by the vector. In practice, the CAV may represent several concepts – *e.g.*, continuing the example above, the vector may encode both **striped** and **red** simultaneously. We refer to this phenomenon as *concept entanglement*. Mathematically, we formulate this as follows. A concept vector $\mathbf{v}_{c,l}$ is more similar to the activations corresponding to images containing the concept than activations for images not containing the concept, *i.e.* it satisfies

$$\mathbf{a}_{c,l}^+ \cdot \mathbf{v}_{c,l} > \mathbf{a}_{c,l}^- \cdot \mathbf{v}_{c,l} \quad \forall \mathbf{a}_{c,l}^+ \in \mathbb{A}_{c,l}^+, \mathbf{a}_{c,l}^- \in \mathbb{A}_{c,l}^- \quad (5)$$

Assume we have concepts c_1 and c_2 , with probe datasets \mathbb{D}_{c_1} and \mathbb{D}_{c_2} , respectively. For each probe dataset, we find the activation sets: $\mathbb{A}_{c_1,l} = \{A_{c_1,l}^+ \cup A_{c_1,l}^-\}$ and $\mathbb{A}_{c_2,l} = \{A_{c_2,l}^+ \cup A_{c_2,l}^-\}$.

Definition 2 (entangled concepts). A CAV $\mathbf{v}_{c_1,l}$ for concept c_1 is entangled with concept c_2 iff

$$\mathbf{a}_{c_2,l}^+ \cdot \mathbf{v}_{c_1,l} > \mathbf{a}_{c_2,l}^- \cdot \mathbf{v}_{c_1,l} \quad \forall \mathbf{a}_{c_2,l}^+ \in \mathbb{A}_{c_2,l}^+, \mathbf{a}_{c_2,l}^- \in \mathbb{A}_{c_2,l}^- \quad (6)$$

Our second hypothesis explores concept entanglement:

Null Hypothesis 2 (NH2): A CAV represents only the concept corresponding to the concept label of its probe dataset

If concepts are entangled, it is not possible to separate the model’s sensitivity to one concept from its sensitivity to related concepts – therefore, if we measure the TCAV score for c_1 , we will unknowingly incorporate the effect of c_2 .

In §6.2 we provide a visualisation tool to explore CAV entanglement and discuss how this can affect TCAV.

3.3 Spatial Dependence

Here, we explore the influence of spatial dependence on concepts. Let \mathbb{D}_{c,μ_1} and \mathbb{D}_{c,μ_2} denote two datasets containing the same concept but in different locations $\mu_1 \neq \mu_2$. For example, \mathbb{D}_{c,μ_1} may contain exemplars of **striped on the left** of the image, and \mathbb{D}_{c,μ_2} exemplars of the **striped on the right** of the image – an example is shown in Fig. 2. As before, we construct latent representations \mathbb{A}_{c,l,μ_1} and \mathbb{A}_{c,l,μ_2} for datasets \mathbb{D}_{c,μ_1} and \mathbb{D}_{c,μ_2} , respectively. Let $\mathbf{v}_{c,l}$ be the concept vector found using probe dataset \mathbb{D}_{c,μ_1} .

Definition 3 (activation spatial dependence). Let $\mathbf{a}_{l,i}$ be the activations corresponding to input \mathbf{x}_i in layer l , and let $\mu_{c,i}$ be the location of concept c in \mathbf{x}_i . A layer has a spatially dependent representation of a concept iff

$$\exists \phi : \forall \mathbf{x}_i \in \mathbb{X}_c^+, \phi(\mathbf{a}_{l,i}) = \mu_{c,i} \quad (7)$$

Activation spatial dependence in a NN may be due to architecture design, training procedure and/or the training dataset. In CNNs, it is the natural consequence of the receptive field of convolutional filters containing different regions of the input. If the NN has spatially dependent activations and the probe dataset has a spatial dependence, it may be possible to create a concept vector with spatial dependence.

Definition 4 (concept vector spatial dependence). A concept vector $\mathbf{v}_{c,l}$ is spatially dependent with respect to the locations μ_1 and μ_2 iff

$$\mathbf{a}_{c,l,\mu_1}^+ \cdot \mathbf{v}_{c,l} > \mathbf{a}_{c,l,\mu_2}^+ \cdot \mathbf{v}_{c,l} \quad \forall \mathbf{a}_{c,l,\mu_1}^+ \in \mathbb{A}_{c,l,\mu_1}^+, \mathbf{a}_{c,l,\mu_2}^+ \in \mathbb{A}_{c,l,\mu_2}^+ \quad (8)$$

If a CAV is spatially dependent then, by the definition above, it is more similar to the activations from images containing the concept in a specific location. This means the CAV represents not only the concept label, but the concept label at a specific location, *e.g.* striped objects on the right of the image, rather than striped objects in general. As done for the other two properties, we propose a hypothesis and aim to reject it later in the paper:

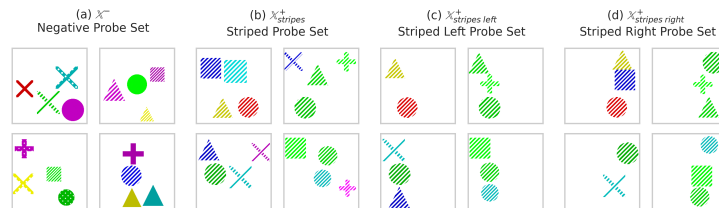


Fig. 2: Example images from Elements probe datasets. (a) Negative probe set. A random selection of images – equivalent to images found in the model training set. (b) Positive probe set for **stripes**. (c) Positive probe set for **stripes on the left**. (d) Positive probe set for **stripes on the right**.

Null Hypothesis 3 (NH3): Concept activation vectors cannot be spatially dependent

We reject this hypothesis in §6.3 by analysing how the concept location in the probe dataset influences the spatial dependence of concept vectors. Rejecting NH3 motivates the introduction of *spatially dependent CAVs* (§ 6.3), which can be used to test if a model is translation invariant with respect to a specific concept and class.

4 Elements: A configurable synthetic dataset

To explore these hypotheses, we introduce a new synthetic dataset: Elements. In this dataset we can control: (1) the training dataset and class definitions, allowing us to influence model properties, such as concept correlation in the embedding space, and (2) the probe dataset, allowing us to test concept vector properties, such as concept vector spatial dependence. We further elaborate on these advantages in Appendix 12.

Figure 2 shows examples of images in the Elements datasets. Each image contains n elements, where an element is defined by seven properties: colour, brightness, size, shape, texture, texture shift, and coordinates within the image. The dataset can be configured by varying the allowed combination of properties for each element. The ranges and configurations used for each property is given in Appendix 12.

5 Related Work

Concept Correlation and Entanglement Chen *et al.* [7] discuss how concept vectors can be correlated, making it challenging to create a vector that solely represents one concept. While their work focuses on de-correlating concepts *during training*, we focus on analysing the impact of correlated concepts *after training* and show how they can lead to misleading explanations (§6.2). Fong and Vedaldi [15] use cosine similarity to demonstrate that the similarity between concepts varies based on the vector creation method. In our work, we also use

cosine similarity to compare concept vectors. The distinction lies in our focus on CAVs and the insights they provide into the dataset and model.

Spatial Dependence Biscione and Bowers [6] describe how CNNs are not inherently translation invariant but can learn to be (under certain conditions on the dataset). This finding challenges the common assumption that CNNs possess inherent translation invariance. Through *spatially dependent CAVs*, we demonstrate translation invariance with respect to a specific concept and class, rather than in general, providing more detailed information about a model.

What concept representations does our analysis apply to? Most concept-based interpretability methods represent concepts as *vectors* in the activation space of a trained neural network (NN) [14, 15, 17, 23, 35, 48, 50]. However, some concept-based methods use different representations: individual neurons [5], regions of activation space [11] or non-linear concepts [4, 26]. Our work focuses on the properties of concept *vectors*.

How is our work relevant in practice? To give insight into when the various properties may be relevant, we performed a review of computer vision papers which use CAVs in (1) the high-stakes applications of medical imaging (including skin cancer, skin lesions, breast cancer, and histology [16, 33, 42]), and (2) computer vision research on models trained with well-known datasets [12, 25, 27, 36, 40, 49]. A summary table can be found in Appendix 16. We found that the following papers could have benefited from evaluating: consistency [16, 18, 28, 34, 42, 45], entanglement [16, 18, 19, 28, 29, 33, 34, 42, 45], and spatial dependence [16, 18, 28, 29, 33, 34, 42, 45]. We provide a detailed example, using the application of skin cancer diagnosis [42], in § 7 and Appendix 17.

Datasets While several datasets have been introduced for evaluating interpretability methods, they differ from ours in a few key ways. There are three aspects we care about:

1. Is the concept represented in the network?
2. Is the concept used for the network’s prediction?
3. How does the network represent correlated concepts?

Existing datasets only allow insight into (1), whereas our dataset allows us to analyse (2) and (3) as well. The Benchmarking Interpretability Method (BIM) [43] inserts objects into scene images. While it benefits from utilizing real images and complex concepts (dog or bedroom), it also presents challenges. One drawback is that relying on real images makes it challenging to establish the ground truth relationship between concepts and class predictions or to know the similarities between concepts. As such, it does not give us insight into (2) or (3). The synthetic dataset in Yeh *et al.* [44] is the most similar to our dataset but was designed for concept discovery, featuring images where each object corresponds to a single concept (shape). In our dataset, each object contains multiple concepts, allowing us to create associations between them. We focus on explanation faithfulness by ensuring that the concepts must be used correctly by the model

to achieve a high accuracy. So, for an accurate model, we have a ground truth understanding of how each concept is used. An extended literature review can be found in Appendix 16.

6 Results: Exploring Concept Vector Properties

We explore the hypotheses on consistency (NH1), entanglement (NH2) and spatial dependency (NH3) in § 6.1, § 6.2 and § 6.3, respectively. We perform experiments using CAVs on the Elements and ImageNet datasets. Implementation details can be found in Appendix 11.

6.1 Consistent CAVs

Theory We begin investigating NH1, which states that CAVs are consistent across layers, *i.e.* $f(\mathbf{a}_{l_1} + \mathbf{v}_{c,l_2}) = \mathbf{a}_{l_2} + \mathbf{v}_{c,l_2}$. Let $\hat{\mathbf{a}}_{l_1}$ and $\hat{\mathbf{a}}_{l_2}$ be linear perturbations to the activations in layers l_1 and l_2 , respectively:

$$\hat{\mathbf{a}}_{l_1} = \mathbf{a}_{l_1} + \mathbf{v}_{c,l_1} \quad (9)$$

$$\hat{\mathbf{a}}_{l_2} = \mathbf{a}_{l_2} + \mathbf{v}_{c,l_2} = f(\mathbf{a}_{l_1}) + \mathbf{v}_{c,l_2} \quad (10)$$

We want to investigate if \mathbf{v}_{c,l_1} and \mathbf{v}_{c,l_2} have the same effect on the activations (and hence the model), *i.e.* if:

$$\begin{aligned} f(\hat{\mathbf{a}}_{l_1}) &= \hat{\mathbf{a}}_{l_2} \\ f(\mathbf{a}_{l_1} + \mathbf{v}_{c,l_1}) &= f(\mathbf{a}_{l_1}) + \mathbf{v}_{c,l_2}. \end{aligned} \quad (11)$$

Assume we have found \mathbf{v}_{c,l_1} and would like to find a \mathbf{v}_{c,l_2} that satisfies Eq. 11. If f conserves vector addition, such as for a linear layer, then it holds that:

$$\begin{aligned} f(\mathbf{a}_{l_1}) + f(\mathbf{v}_{c,l_1}) &= f(\mathbf{a}_{l_1}) + \mathbf{v}_{c,l_2} \\ \mathbf{v}_{c,l_2} &= f(\mathbf{v}_{c,l_1}). \end{aligned} \quad (12)$$

Hence, it is possible to have consistent vectors across layers if f conserves vector addition and $\mathbf{v}_{c,l_2} = f(\mathbf{v}_{c,l_1})$. Alternatively, if f does not conserve vector addition, we cannot simplify Eq. 11 and for a given \mathbf{v}_{c,l_1} :

$$\mathbf{v}_{c,l_2} = f(\mathbf{a}_{l_1} + \mathbf{v}_{c,l_1}) - f(\mathbf{a}_{l_1}). \quad (13)$$

If \mathbf{v}_{c,l_2} depends on \mathbf{a}_{l_1} , there does not exist a \mathbf{v}_{c,l_2} such that Eq. 11 is true for all \mathbf{a}_{l_1} . In other words, there does not exist a vector in layer l_2 which has the same effect on the activations as the vector in layer l_1 for all inputs to the model.

ReLU and sigmoid functions are common NN activations. Using Eq. 13, for any input i , if

$$f = \text{ReLU} : \quad a_{l_1,i} + v_{l_1,i} > 0, \quad a_{l_1,i} \leq 0, \quad \text{or} \quad a_{l_1,i} + v_{l_1,i} \leq 0, \quad a_{l_1,i} > 0 \quad (14)$$

$$f = \text{sigmoid} : \quad v_{l_1,i} \neq 0 \quad (15)$$

then there does not exist a consistent \mathbf{v}_{c,l_2} , *i.e.* it is **impossible** to have consistent vectors under these conditions. The proofs for Eqs. (14) and (15) are available in Appendix 10. Next, we demonstrate that we cannot find consistent vectors in practice.

Experiments Our goal is to investigate the question *are the concept vectors found using TCAV consistent?* We measure the consistency of two perturbations using the consistency error:

$$\epsilon_{consistency} = \|f(\hat{\mathbf{a}}_{l_1}) - \hat{\mathbf{a}}_{l_2}\| = \|f(\mathbf{a}_{l_1} + \mathbf{v}_{c,l_1}) - (\mathbf{a}_{l_2} + \mathbf{v}_{c,l_2})\| \quad (16)$$

In our experiments, we use a scaling term to reduce the size of \mathbf{v}_{c,l_1} and \mathbf{v}_{c,l_2} to ensure the perturbed activation remains in distribution – see Appendix 13.1 for details. If two perturbations have a consistency error of 0, then they have the same effect on the model. We include the following benchmarks:

Optimised CAV (lower bound): TCAV may not find a \mathbf{v}_{c,l_2} that has a consistency error of 0 with \mathbf{v}_{c,l_1} . Therefore, we use gradient decent on \mathbf{v}_{c,l_2} to minimise the consistency error, which acts as a lower bound.

Projected CAV : the error between $f(\mathbf{v}_{c,l_1})$ and \mathbf{v}_{c,l_2} , which measures how consistent the vectors are when projected into the next layer. If $f(\cdot)$ conserves vector addition, the projected CAVs would have 0 error.

Random (upper bound): We include two benchmarks. Random CAVs found using probe datasets containing random images, and a Random Direction vector: $\mathbf{v}_{c,l_2} \sim \text{Uniform}(-1, 1)$. If the consistency error is similar to random, it suggests that the CAVs between layers are as similar to each other as random directions.

Fig. 3 shows the $\epsilon_{consistency}$ for different \mathbf{v}_{c,l_2} across different training runs (see Appendix 13 for details). The concept CAV obtains a nonzero consistency error, suggesting that CAVs across different layers are not consistent. When we compare it with the benchmarks, we find:

- The consistency error for the optimised CAVs is lower, implying that the standard approach to find CAVs does not find optimally consistent CAVs. However, the nonzero error for optimised CAVs suggests it is not possible to find consistent vectors in these layers.
- The projected CAVs have a nonzero error, indicating that vector addition is not preserved.
- The random CAVs have a higher error, suggesting the concept CAVs are more similar than random vectors.

The inability to find consistent concept vectors across layers suggests that the directions encoded by CAVs in different layers are not equivalent; instead we speculate that they represent different components of the same concept. This aligns with the intuition that model representations are more complex later in the NN [5, 30, 32], therefore it is unlikely that the same aspects of a concept are represented in different layers (discussed further in Appendix 13.3). Consequently, TCAV scores across layers can vary as they perform different tests – they measure the class sensitivity to a different version of the concept.

Fig. 5c shows that concept vectors found in different layers of a model can give contradictory TCAV scores (further examples available in Appendix 13.4). In the Elements dataset, shape concepts are encoded in each layer as the test accuracy

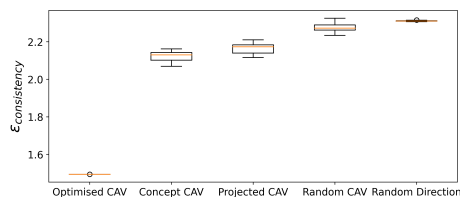


Fig. 3: Empirical evidence for inconsistent CAVs. The consistency error for different \mathbf{v}_{c,l_2} for **striped** in the penultimate convolutional layer of a ResNet-50 trained on ImageNet. The optimised CAV acts as lower bound, whereas the random CAV and Direction act as baselines that provide an intuitive upper bounds. Concept CAV: **striped** CAVs, trained as normal. Projected CAV: **striped** CAVs from layer l_1 projected into layer l_2 , $f(\mathbf{v}_{c,l_1})$.

for each layer is above 93%. Therefore, we expect to be able to use TCAV on each of these layers. However, the TCAV scores for **cross** in the Elements dataset contradict each other across ‘layers.3’ and ‘layers.4’, suggesting a positive and negative influence, respectively. This contradiction makes it difficult to draw a conclusion about the model’s class sensitivity to **cross**.

On the right of Fig. 5c, we show the TCAV scores for **striped** for various classes in a ResNet-50 model trained on ImageNet. The accuracy for the **striped** vectors in ImageNet is above 96% for all layers tested, suggesting that the concept is encoded by the model in each of the layers. As in Elements, we do not observe consistent TCAV scores across layers. Instead, we observe a large change in the TCAV scores for **striped** in the penultimate layer, compared to earlier layers. ‘layer4.1’ suggests **striped** positively influences the likelihood of the classes tiger and leopard. However, earlier layers suggest that the class is not sensitive to the concept. This shows how, depending on the layers that are tested, different conclusions can be drawn.

6.2 Entanglement

Different concepts may be associated with each other. For example, consider **blue** and the **sky** – a fundamental aspect of the sky is that it is often blue. These concepts are inherently linked and should not be treated as independent. This section will discuss how to discover these associations using CAVs and the implications for TCAV.

To explore entanglement, we quantify and visualize concept associations by computing average pairwise cosine similarities between CAVs (we compute multiple CAVs for each concept). We investigate three models trained on different versions of the Elements dataset. Each dataset is identical aside from the association between **red** and **triangle**:

- \mathbb{E}_1 : each combination of colour, shape and texture is equally likely,
- \mathbb{E}_2 : the only shape that is red is triangles,
- \mathbb{E}_3 : the concepts of red and triangle only ever co-occur.

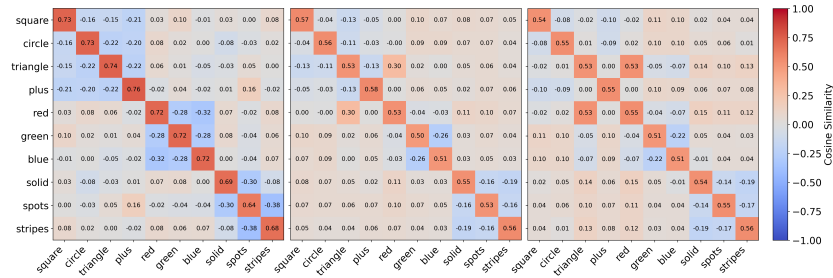


Fig. 4: Cosine similarities demonstrating entangled concepts. Mean pairwise cosine similarities for all concepts from different versions of the simple Elements dataset, with an increasing association between **red** and **triangle** from left to right: \mathbb{E}_1 , \mathbb{E}_2 and \mathbb{E}_3 .

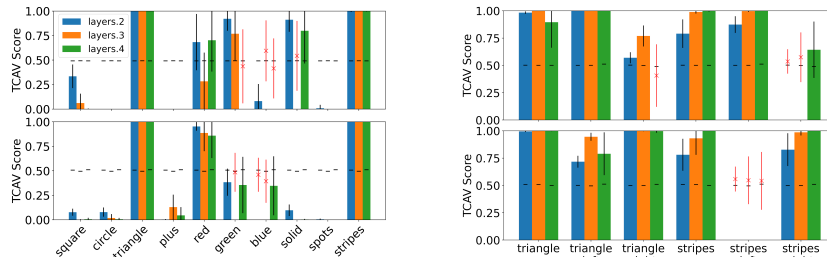
In Fig. 4 we show one plot for each dataset. For \mathbb{E}_1 , we observe no positive association between the concepts. In \mathbb{E}_2 , we observe a small positive association between the triangle and red concepts. Lastly, in \mathbb{E}_3 , the cosine similarity between the **red** and **triangle** CAVs approaches the similarity of the concept with itself. The trend between \mathbb{E}_1 , \mathbb{E}_2 and \mathbb{E}_3 is likely due to the underlying association between the **red** and **triangle** increasing. We perform similar analyses on ImageNet in Appendix 14.

Interestingly, we often observe a negative cosine similarity between mutually exclusive concepts. The model has encoded concepts that cannot co-occur (*e.g.*, each element can only have a single colour) in directions negatively correlated with each other. The presence of the **red** diminishes the likelihood of the **blue** or **green** being present, and by having these concepts negatively associated with each other the model builds in this reasoning. This means that the **red** CAV does not solely signify **red**, it also encapsulates **not blue** and **not green**.

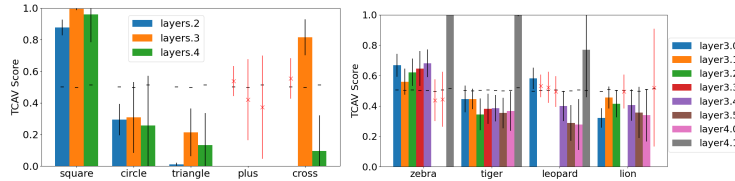
Next, we investigate the effect of entangled concept vectors on TCAV score. We analyse the TCAV scores for the ‘striped triangles’ class in \mathbb{E}_1 and \mathbb{E}_2 . The class label depends solely on the presence **stripes** and **triangle**. Therefore, we expect all other concepts to obtain low TCAV scores (indicating negative sensitivity), as their presence makes the class less likely, or insignificant TCAV scores, if the concept is uninformative.⁴

The results for \mathbb{E}_1 and \mathbb{E}_2 are shown on the top and bottom of Fig. 5a, respectively. For \mathbb{E}_1 (the unaltered dataset), we find that only the **stripes** and **triangle** vectors have a high TCAV score across multiple layers. For \mathbb{E}_2 (the altered dataset), however, the model appears to be sensitive to **red**, **triangle** and **stripes**, with high TCAV scores for each. This is due to the association between the **red** and **triangle** CAVs. 2,374/5,000 images in the test dataset contain striped triangles. None of these are incorrectly classified, so it is unlikely that the model uses the red concept for its prediction. Instead, the association between CAVs causes a misleadingly high TCAV score for the red concept. In conclusion, associated CAVs can lead to misleading explanations.

⁴ assuming that the model uses each concept correctly



(a) Entangled CAVs increase red TCAV scores for \mathbb{E}_2 . TCAV scores for all concepts in \mathbb{E}_1 (top) and \mathbb{E}_2 (bot) for the class of striped triangles.



(c) Inconsistent TCAV scores across layers. Left: TCAV scores for shape concepts for the ‘solid red squares’ class in Elements. Right: TCAV scores for striped for a subset of ImageNet classes.

Fig. 5: Consistency, entanglement, spatial dependence can affect TCAV scores. The standard deviation is black or red for significant and insignificant results, respectively. The null for each layer is shown as a horizontal black line.

6.3 Spatial Dependence

Finally, we investigate NH3: *are CAVs spatially dependent?* We reshape the CAVs back into the original shape of the activations, and compute the channel-wise norm as follows:

$$\mathbf{S}_{c,l} = \|\text{reshape}(\mathbf{v}_{c,l}, (H, W, D))\|_2, \quad (17)$$

where $\mathbf{S}_{c,l} \in \mathbb{R}^{H \times W}$, and $\|\cdot\|_2$ is the L_2 norm across the channel dimension. We refer to this array as the spatial norms of the CAV.

If a CAV’s spatial norm varies substantially across the (H, W) dimensions, it indicates that the CAV is spatially dependent (see Appendix 15.2 for an explanation). Visualising a CAV’s spatial norms shows us which regions contribute most to the directional derivative and, consequently, to the TCAV score.

To create spatially dependent CAVs, we constructed spatially dependent probe datasets for Elements and ImageNet where we either restricted the location of the concepts or greyed out parts of the image – see Fig. 2 for examples and Appendix 15.1 for further details.

When a spatially independent probe dataset is used to create CAVs, as in the top row of Fig. 6, the spatial norms are uniform, suggesting the CAVs are not spatially dependent⁵. However, when the probe dataset exhibits spatial dependence, so do the resulting CAVs. The regions of near-zero norm indicate

⁵ the individual CAVs may still be spatially dependent, but this cancels out across training runs. See Appendix 15.3 for details.

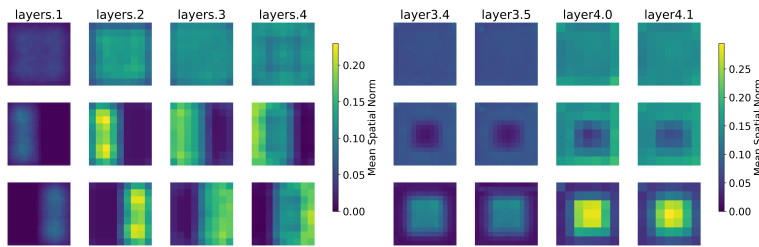


Fig. 6: Spatial norms reflect the spatial dependence of the probe dataset. Left: Mean spatial norms for **red** (top), **red left** (middle) and **red right** (bottom) for Elements. Right: Mean spatial norms across for **striped** (top), **striped edges** (middle) and **striped middle** (bottom) for ImageNet.

that the corresponding spatial regions of the gradients do not contribute to the directional derivative and, consequently, to the TCAV score.

Next, we investigate the question *does the model have a different conceptual sensitivity depending on the concepts location in the input image?* As CAVs operate in the activation space of a specific layer, we can show that model is not translation invariant if:

1. The model has activation spatial dependence, *i.e.* pixels in different locations affect the activations differently.
2. That each depth-wise slice of the activations, of shape $(1, 1, D)$, affects the logit output differently.

Both of these components affect the TCAV score. (1) influences $\mathbf{v}_{c,l}$ and (2) influences $\nabla h_{l,k}(g_l(\mathbf{x}))$. For (1), Fig. 6 demonstrates that the model has activation spatial dependence as the locations with the highest spatial norms approximately correspond to the location of the concept in the image space.

To address (2), we compute the TCAV scores for different sets of spatially dependent CAVs to determine if the sensitivity of the model changes depending on the concepts location. To investigate this, we created spatially dependent classes in the Elements dataset, where the class depends on what concepts are present *and* on where they are in the image, such as ‘striped triangles on the left’. We use spatially dependent CAVs to show that a model is not translation invariant with respect to **striped** or **triangle** in Fig. 5b. Here, we discuss the results for the class of ‘striped triangles on the left’. The TCAV scores for **striped**, **triangle**, **striped left** and **triangle left** are high, indicating a positive influence of these concepts on the class. However, the **striped right** and **triangle right** TCAV scores often do not differ significantly from the null scores, providing no evidence to suggest the model is sensitive to these concepts. The difference between the left and right biased TCAV scores indicates that the model is not translation invariant with respect to these concepts as the model’s sensitivity depends on where the concept is present in the image input space. Overall, this suggests that we can use CAVs to detect model translation invariance. See Appendix 15.6 for examples on ImageNet.

7 Practitioner Recommendations

Our results have shown that failure to appropriately consider consistency, entanglement, and spatial dependence may result in drawing incorrect conclusions when using TCAV. Therefore, we recommend the following:

- *Consistency*: creating CAVs for multiple layers, rather than a single one;
- *Entanglement*: (1) verifying expected dependencies between related concepts, and (2) being mindful that a positive TCAV score may be due to concept entanglement;
- *Spatial Dependence*: visualising concept vector spatial dependence using spatial norms.

In Section 5, we provided example papers which use CAVs and may be influenced by the above properties. As a more concrete example, we examine the use-case of Yan *et al.* [42] which uses CAVs in the context of skin cancer diagnosis. Some of the concepts have expected spatial dependencies, for example, **dark borders** and **dark corners**. Spatial norms could be used to confirm these spatial dependencies exist. Equally, for concepts such as the presence of a **ruler**, the spatial norms could confirm the CAVs have no overall spatial dependence. There are multiple concepts which have opposed meanings, for example **regular streaks** and **irregular streaks**. The cosine similarities between CAVs could confirm that these concepts are negatively correlated or at least less similar to each other than to other concepts. We provide a more detailed analysis of this use-case in Appendix 17.

8 Conclusion and Future Work

In this work, we explore three key properties that influence concept activation vectors (CAVs): consistency, entanglement and spatial dependence. First, we derive conditions under which CAVs in different layers are not consistent and substantiate our findings with empirical evidence. This sheds light on why CAV-based explanations methods can give conflicting conclusions across layers. Next, we introduce a visualisation tool designed to facilitate the exploration of associations between concepts within a dataset and model. Lastly, we show that spatial dependence impacts CAVs, and introduce a method that can be used to detect spatial dependence within models. Each of these experiments was conducted using a synthetic dataset, Elements, where custom probe datasets can easily be created to analyse properties of interest. We release this dataset to help further explore this problem space.

In the introduction, we cited several interpretability methods that employ vector representations to convey semantically meaningful concepts. Our study has illuminated certain properties and consequential outcomes arising from these vector-based approaches. In future research, the characteristics inherent in alternative forms of representation, such as clusters within activation space [11], should be investigated and the relative merits assessed.

9 Acknowledgements

We appreciate both the members of OATML and the Noble group for your support and discussions during the project, in particular Andrew Jesson. We are also grateful to Been Kim for your thoughts and feedback on our work. A. Nicolson is supported by the EPSRC Centre for Doctoral Training in Health Data Science (EP/S02428X/1). J.A. Noble acknowledges EPSRC grants EP/X040186/1 and EP/T028572/1.

References

1. Achibat, R., Dreyer, M., Eisenbraun, I., Bosse, S., Wiegand, T., Samek, W., Lapuschkin, S.: From "where" to "what": Towards human-understandable explanations through concept relevance propagation (2022) [1](#)
2. Adebayo, J., Gilmer, J., Muelly, M., Goodfellow, I., Hardt, M., Kim, B.: Sanity checks for saliency maps. In: *Advances in Neural Information Processing Systems*. pp. 9525–9536 (2018) [1](#)
3. Alain, G., Bengio, Y.: Understanding intermediate layers using linear classifier probes. *International Conference on Learning Representations* (2017) [49](#)
4. Bai, A., Yeh, C.K., Ravikumar, P., Lin, N.Y.C., Hsieh, C.J.: Concept gradient: Concept-based interpretation without linear assumption (2022) [7](#)
5. Bau, D., Zhou, B., Khosla, A., Oliva, A., Torralba, A.: Network dissection: Quantifying interpretability of deep visual representations. In: *Proceedings of the IEEE Conference on Computer Vision and Pattern Recognition*. pp. 6541–6549 (2017) [7](#), [9](#), [22](#)
6. Biscione, V., Bowers, J.S.: Convolutional neural networks are not invariant to translation, but they can learn to be. *Journal of Machine Learning Research* **22**(229), 1–28 (2021) [7](#)
7. Chen, Z., Bei, Y., Rudin, C.: Concept whitening for interpretable image recognition. *Nature Machine Intelligence* **2**, 772 – 782 (2020) [6](#)
8. Codella, N.C.F., Gutman, D., Celebi, M.E., Helba, B., Marchetti, M.A., Dusza, S.W., Kalloo, A., Liopyris, K., Mishra, N., Kittler, H., Halpern, A.: Skin lesion analysis toward melanoma detection: A challenge at the 2017 international symposium on biomedical imaging (isbi), hosted by the international skin imaging collaboration (isic) (2017) [50](#)
9. Colin, J., FEL, T., Cadene, R., Serre, T.: What i cannot predict, i do not understand: A human-centered evaluation framework for explainability methods. In: Oh, A.H., Agarwal, A., Belgrave, D., Cho, K. (eds.) *Advances in Neural Information Processing Systems* (2022) [1](#)
10. Combalia, M., Codella, N.C.F., Rotemberg, V., Helba, B., Vilaplana, V., Reiter, O., Halpern, A.C., Puig, S., Malvehy, J.: Bcn20000: Dermoscopic lesions in the wild (2019) [50](#)
11. Crabbé, J., van der Schaar, M.: Concept activation regions: A generalized framework for concept-based explanations. In: *Advances in Neural Information Processing Systems*. vol. 35, pp. 2590–2607 (2022) [7](#), [14](#)
12. Deng, J., Dong, W., Socher, R., Li, L.J., Li, K., Fei-Fei, L.: Imagenet: A large-scale hierarchical image database. In: *CVPR*. pp. 248–255 (2009). <https://doi.org/10.1109/CVPR.2009.5206848> [4](#), [7](#), [49](#)

13. Elhage, N., Hume, T., Olsson, C., Schiefer, N., Henighan, T., Kravec, S., Hatfield-Dodds, Z., Lasenby, R., Drain, D., Chen, C., Grosse, R., McCandlish, S., Kaplan, J., Amodei, D., Wattenberg, M., Olah, C.: Toy models of superposition (2022) [41](#)
14. Fel, T., Picard, A., Bethune, L., Boissin, T., Vigouroux, D., Colin, J., Cadène, R., Serre, T.: Craft: Concept recursive activation factorization for explainability. *CVPR* (2023) [7](#)
15. Fong, R., Vedaldi, A.: Net2vec: Quantifying and explaining how concepts are encoded by filters in deep neural networks. *CoRR* [abs/1801.03454](#) (2018) [6](#), [7](#)
16. Fürböck, C., Perkonig, M., Helbich, T., Pinker, K., Romeo, V., Langs, G.: Identifying Phenotypic Concepts Discriminating Molecular Breast Cancer Sub-Types. In: *MICCAI* (2022) [7](#), [49](#)
17. Ghorbani, A., Wexler, J., Zou, J., Kim, B.: Towards automatic concept-based explanations. In: *Advances in Neural Information Processing Systems* (2019) [7](#), [49](#)
18. Ghosh, S., Yu, K., Arabshahi, F., Batmanghelich, K.: Dividing and conquering a blackbox to a mixture of interpretable models: Route, interpret, repeat. In: *ICML* (2023) [7](#), [49](#)
19. Graziani, M., Andrearczyk, V., S., M.M., Müller, H.: Concept attribution: Explaining CNN decisions to physicians. *Computers in Biology and Medicine* **123** (Aug 2020) [7](#), [49](#)
20. He, K., Zhang, X., Ren, S., Sun, J.: Deep residual learning for image recognition. In: *Proceedings of the IEEE Computer Society Conference on Computer Vision and Pattern Recognition*. pp. 770–778 (2016) [22](#)
21. Hoffer, E., Ben-Nun, T., Hubara, I., Giladi, N., Hoefler, T., Soudry, D.: Augment Your Batch: Improving Generalization Through Instance Repetition. In: *IEEE/CVF Conference on Computer Vision and Pattern Recognition (CVPR)*. pp. 8126–8135 (2020) [22](#)
22. Kawahara, J., Daneshvar, S., Argenziano, G., Hamarneh, G.: Seven-point checklist and skin lesion classification using multitask multimodal neural nets. *IEEE Journal of Biomedical and Health Informatics* **23**(2), 538–546 (2019). <https://doi.org/10.1109/JBHI.2018.2824327> [50](#)
23. Kim, B., Wattenberg, M., Gilmer, J., Cai, C., Wexler, J., Viegas, F., et al.: Interpretability beyond feature attribution: Quantitative testing with concept activation vectors (TCAV). In: *International Conference on Machine Learning*. pp. 2668–2677. *PMLR* (2018) [2](#), [3](#), [7](#), [21](#)
24. Kingma, D.P., Ba, J.: Adam: A method for stochastic optimization. In: *International Conference on Learning Representations* (2015) [21](#), [50](#)
25. Krizhevsky, A.: Learning multiple layers of features from tiny images (2009) [7](#), [49](#)
26. Li, K., Hopkins, A.K., Bau, D., Viégas, F., Pfister, H., Wattenberg, M.: Emergent world representations: Exploring a sequence model trained on a synthetic task (2023) [7](#)
27. Lin, T., Maire, M., Belongie, S.J., Bourdev, L.D., Girshick, R.B., Hays, J., Perona, P., Ramanan, D., Dollár, P., Zitnick, C.L.: Microsoft COCO: common objects in context. *CoRR* [abs/1405.0312](#) (2014) [7](#), [49](#)
28. Lucieri, A., Bajwa, M.N., Braun, S.A., Malik, M.I., Dengel, A., Ahmed, S.: On interpretability of deep learning based skin lesion classifiers using concept activation vectors. In: *IJCNN* (2020) [7](#), [49](#)
29. McGrath, T., Kapishnikov, A., Tomašev, N., Pearce, A., Wattenberg, M., Hassabis, D., Kim, B., Paquet, U., Kramnik, V.: Acquisition of chess knowledge in alphazero. *Proceedings of the National Academy of Sciences* **119**(47) (Nov 2022). <https://doi.org/10.1073/pnas.2206625119> [7](#), [24](#)

30. Mordvintsev, A., Olah, C., Tyka, M.: Inceptionism: Going deeper into neural networks. Google Research Blog (2015), retrieved November 2017 [9](#), [34](#)
31. Müller, S.G., Hutter, F.: Trivialaugment: Tuning-free yet state-of-the-art data augmentation. In: 2021 IEEE/CVF International Conference on Computer Vision (ICCV). pp. 754–762. ICCV (2021) [22](#)
32. Olah, C., Mordvintsev, A., Schubert, L.: Feature visualization. Distill **2**(11), e7 (2017) [9](#)
33. Pfau, J., Young, A.T., Wei, J., Wei, M.L., Keiser, M.J.: Robust Semantic Interpretability: Revisiting Concept Activation Vectors. In: ICML WHI (2020) [7](#), [49](#)
34. Ramaswamy, V.V., Kim, S.S.Y., Fong, R.C., Russakovsky, O.: Overlooked factors in concept-based explanations: Dataset choice, concept learnability, and human capability. 2023 IEEE/CVF Conference on Computer Vision and Pattern Recognition (CVPR) pp. 10932–10941 (2022) [2](#), [7](#), [48](#), [49](#)
35. Ramaswamy, V.V., Kim, S.S.Y., Meister, N., Fong, R., Russakovsky, O.: Elude: Generating interpretable explanations via a decomposition into labelled and unlabelled features (2022) [7](#)
36. Sagawa, S., Koh, P.W., Hashimoto, T.B., Liang, P.: Distributionally Robust Neural Networks for Group Shifts: On the Importance of Regularization for Worst-Case Generalization (2020) [7](#), [49](#)
37. Schrouff, J., Baur, S., Hou, S., Mincu, D., Loreaux, E., Blanes, R., Wexler, J., Karthikesalingam, A., Kim, B.: Best of both worlds: local and global explanations with human-understandable concepts. ArXiv [abs/2106.08641](#) (2021) [49](#)
38. Soni, R., Shah, N., Seng, C.T., Moore, J.D.: Adversarial tcav - robust and effective interpretation of intermediate layers in neural networks. ArXiv [abs/2002.03549](#) (2020) [2](#), [48](#)
39. Tschandl, P., Rosendahl, C., H., K.: The ham10000 dataset, a large collection of multi-source dermatoscopic images of common pigmented skin lesions. Sci. Data **5**, 180161 (2018) [50](#)
40. Wah, C., Branson, S., Welinder, P., Perona, P., Belongie, S.: The caltech-ucsd birds-200-2011 dataset. Computation & Neural Systems Technical Report (2011) [7](#), [49](#)
41. Xu, Y., Zhao, S., Song, J., Stewart, R., Ermon, S.: A theory of usable information under computational constraints (2020) [24](#)
42. Yan, S., Yu, Z., Zhang, X., Mahapatra, D., Chandra, S.S., Janda, M., Soyer, P., Ge, Z.: Towards trustable skin cancer diagnosis via rewriting model’s decision. In: CVPR (2023) [7](#), [14](#), [49](#), [50](#), [51](#)
43. Yang, M., Kim, B.: BIM: towards quantitative evaluation of interpretability methods with ground truth. CoRR [abs/1907.09701](#) (2019) [7](#)
44. Yeh, C.K., Kim, B., Arik, S., Li, C.L., Pfister, T., Ravikumar, P.: On completeness-aware concept-based explanations in deep neural networks. Advances in Neural Information Processing Systems **33**, 20554–20565 (2020) [7](#)
45. Yuksekgonul, M., Wang, M., Zou, J.: Post-hoc concept bottleneck models. In: ICLR (2023) [7](#), [49](#)
46. Yun, S., Han, D., Chun, S., Oh, S., Yoo, Y., Choe, J.: Cutmix: Regularization strategy to train strong classifiers with localizable features. In: IEEE/CVF International Conference on Computer Vision (ICCV). pp. 6022–6031 (2019) [22](#)
47. Zhang, H., Cisse, M., Dauphin, Y.N., Lopez-Paz, D.: mixup: Beyond empirical risk minimization. In: International Conference on Learning Representations (2018) [22](#)
48. Zhang, R., Madumal, P., Miller, T., Ehinger, K.A., Rubinstein, B.I.P.: Invertible concept-based explanations for cnn models with non-negative concept activation vectors. In: AAAI Conference on Artificial Intelligence (2020) [7](#), [49](#)

49. Zhou, B., Lapedriza, A., Khosla, A., Oliva, A., Torralba, A.: Places: A 10 million Image Database for Scene Recognition. *IEEE Transactions on Pattern Analysis and Machine Intelligence* (2017) 7, 49
50. Zhou, B., Sun, Y., Bau, D., Torralba, A.: Interpretable basis decomposition for visual explanation. In: *Computer Vision – ECCV 2018*. pp. 122–138. Springer International Publishing (2018) 7

Explaining Explainability: Understanding Concept Activation Vectors

Supplementary Material

10 Consistency Proof

Let $\mathbf{a}_{l_1,i}$ be the activation vector in layer l for the input $\mathbf{x}_i \in \mathbb{X}$. Function f projects the activations in layer l_1 to layer l_2 , where $l_1 < l_2$, i.e. $f(\mathbf{a}_{l_1,i}) = \mathbf{a}_{l_2,i}$.

Let $\hat{\mathbf{a}}_{l_1}$ and $\hat{\mathbf{a}}_{l_2}$ be linearly perturbed activations in each of these layers:

$$\hat{\mathbf{a}}_{l_1} = \mathbf{a}_{l_1,i} + \mathbf{u} \quad (18)$$

$$\hat{\mathbf{a}}_{l_2} = \mathbf{a}_{l_2,i} + \mathbf{v} = f(\mathbf{a}_{l_1,i}) + \mathbf{v}, \quad (19)$$

where $\mathbf{u} \in \mathbb{R}^{m_{l_1}}$ and $\mathbf{v} \in \mathbb{R}^{m_{l_2}}$ are perturbation vectors and m_{l_1} and m_{l_2} are the dimensions of layer l_1 and l_2 , respectively. For the two perturbations to have the same effect on the activations (and hence the model) it must hold that:

$$\begin{aligned} f(\hat{\mathbf{a}}_{l_1}) &= \hat{\mathbf{a}}_{l_2} \\ f(\mathbf{a}_{l_1,i} + \mathbf{u}) &= f(\mathbf{a}_{l_1,i}) + \mathbf{v} \end{aligned} \quad (20)$$

Assume we have \mathbf{u} and are aiming to find a \mathbf{v} which satisfies Eq. 20. If f conserves vector addition then

$$\begin{aligned} f(\mathbf{a}_{l_1,i} + \mathbf{u}) &= f(\mathbf{a}_{l_1,i}) + \mathbf{v} \\ f(\mathbf{a}_{l_1,i}) + f(\mathbf{u}) &= f(\mathbf{a}_{l_1,i}) + \mathbf{v} \\ \mathbf{v} &= f(\mathbf{u}) \end{aligned} \quad (21)$$

So, if f conserves vector addition, it is possible to have consistent vectors \mathbf{v} and \mathbf{u} iff $\mathbf{v} = f(\mathbf{u})$.

Alternatively, if f does not conserve vector addition, we cannot simplify Eq. 20. In that case, we get the following solution for \mathbf{v} :

$$\mathbf{v} = f(\mathbf{a}_{l_1,i} + \mathbf{u}) - f(\mathbf{a}_{l_1,i}). \quad (22)$$

If \mathbf{v} depends on i then there does not exist a \mathbf{v} such that Eq. 20 is true for all i .

10.1 ReLU Proof

In a neural network, f often involves a rectified linear unit (ReLU), so below we find \mathbf{v} when $f = \text{ReLU}$. Let $a_{l_1,i,j}$, v_j and u_j refer to the individual elements of $\mathbf{a}_{l_1,i}$, \mathbf{v} and \mathbf{u} , respectively. By the definition of a ReLU activation:

$$f(a_{l_1,i,j}) = \max(0, a_{l_1,i,j}) = \begin{cases} a_{l_1,i,j} & a_{l_1,i,j} > 0 \\ 0 & a_{l_1,i,j} \leq 0 \end{cases} \quad (23)$$

So, Eq. 22 becomes:

$$\begin{aligned}
v_j &= \max(0, a_{l_1, i, j} + u_j) - \max(0, a_{l_1, i, j}) \\
&= \begin{cases} a_{l_1, i, j} + u_j - a_{l_1, i, j} & a_{l_1, i, j} + u_j > 0, a_{l_1, i, j} > 0 \\ a_{l_1, i, j} + u_j + 0 & a_{l_1, i, j} + u_j > 0, a_{l_1, i, j} \leq 0 \\ 0 - a_{l_1, i, j} & a_{l_1, i, j} + u_j \leq 0, a_{l_1, i, j} > 0 \\ 0 - 0 & a_{l_1, i, j} + u_j \leq 0, a_{l_1, i, j} \leq 0 \end{cases} \quad (24) \\
&= \begin{cases} u_j & a_{l_1, i, j} + u_j > 0, a_{l_1, i, j} > 0 \\ a_{l_1, i, j} + u_j & a_{l_1, i, j} + u_j > 0, a_{l_1, i, j} \leq 0 \\ a_{l_1, i, j} & a_{l_1, i, j} + u_j \leq 0, a_{l_1, i, j} > 0 \\ 0 & a_{l_1, i, j} + u_j \leq 0, a_{l_1, i, j} \leq 0. \end{cases}
\end{aligned}$$

If $a_{l_1, i, j} + u_j > 0, a_{l_1, i, j} \leq 0$ or $a_{l_1, i, j} + u_j \leq 0, a_{l_1, i, j} > 0$ for any element j then there does not exist a v such that Eq. 20 is true for all i , *i.e.*, when either of these statements are true, you cannot have two vectors which have the same effect on the activations across layers for all possible inputs.

10.2 Sigmoid Proof

In this section, we consider the sigmoid activation: $f(x) = \frac{1}{1 + \exp(-x)}$. For ease of notation, we drop i and j as they do not change, but a_{l_1} and a_{l_2} refer to $a_{l_1, i, j}$ and $a_{l_2, i, j}$, respectively. From Eq. 20, the concept vectors are consistent iff

$$f(a_{l_1} + u) = f(a_{l_1}) + v \quad (25)$$

$$\frac{1}{1 + \exp(-a_{l_1} - u)} = \frac{1}{1 + \exp(-a_{l_1})} + v \quad (26)$$

Simplifying Eq. 26 for v , we get:

$$\begin{aligned}
v &= \frac{1}{1 + \exp(-a_{l_1} - u)} - \frac{1}{1 + \exp(-a_{l_1})} \\
v &= \frac{(1 + \exp(-a_{l_1})) - (1 + \exp(-a_{l_1} - u))}{(1 + \exp(-a_{l_1}))(1 + \exp(-a_{l_1} - u))} \\
v &= \frac{\exp(-a_{l_1}) - \exp(-a_{l_1} - u)}{(1 + \exp(-a_{l_1}))(1 + \exp(-a_{l_1} - u))} \\
v &= \frac{1 - \exp(-u)}{(\exp(a_{l_1}) + 1)(\exp(a_{l_1}) + \exp(-u))}
\end{aligned}$$

This can be simplified further with partial fractions:

$$v = \frac{1 - \exp(-u)}{(\exp(a_{l_1}) + 1)(\exp(a_{l_1}) + \exp(-u))} \quad (27)$$

$$= \frac{\exp(-a_{l_1})}{(\exp(a_{l_1}) + 1)} - \frac{\exp(-a_{l_1} - u)}{(\exp(a_{l_1}) + \exp(-u))} \quad (28)$$

$$= \frac{\exp(-a_{l_1})}{(\exp(a_{l_1}) + 1)} - \frac{\exp(-a_{l_1})}{(\exp(a_{l_1} + u) + \exp(-u))} \quad (29)$$

For a single v to exist which is consistent for all a_{l_1} it cannot depend on a_{l_1} . Since the left half of Eq. 29 depends on a_{l_1} , the only way that v does not depend on a_{l_1} is if the right hand side cancels out the left. This only occurs when $u = v = 0$. In other words, the only vector which is consistent across a sigmoid function is a vector which has no effect on the activations.

11 Implementation Details

In this section, we provide general implementation details applicable to the whole paper. For details relating to individual experiments and additional results, see Sections 13, 14 and 15.

11.1 Concept Activation Vectors

Background In [23], a statistical test, TCAV, determines whether the model’s sensitivity to a concept is significant. The test compares a set of CAV scores found using a concept dataset with CAV scores found using random data. To do this, we must find multiple CAVs for each concept. In practice, each of these CAVs is trained with the same positive set, \mathbb{X}_c^+ , but a different random set, \mathbb{X}_c^r , where $r \in 1, 2 \dots R$ denotes the random index. A CAV corresponding to a specific random index is labelled $v_{c,l}^r$.

Implementation Details In this work, we create multiple CAVs per training run (30 unless otherwise stated), each using the same positive probe dataset but a different random set. We label a CAV trained with a specific random set as $v_{c,l}^r$, where $r \in 1, 2 \dots R$ denotes the random index. Random CAVs are generated from pairwise combinations of random data sets, and we conduct a two-sided Welch’s t-test to test whether the means of concept and random TCAV scores are equal. If a set of CAVs passes this test with a p value less than 0.01⁶, we consider the concept meaningful. We refer to the mean TCAV score of the random CAVs as the null; it acts as the TCAV score all other CAVs should be compared against to understand their sensitivity to the model. The null is often very close to 0.5, simplifying the interpretation of the TCAV score to the concept having positive sensitivity when greater than 0.5 and negative when less.

11.2 Elements

Classification Model The model architecture is a simple convolutional neural network with six layers: each layer contains a convolution, batch norm and ReLU, followed by an average pooling and fully connected layer to give the logit outputs. The first three convolutional layers utilise a max-pooling operation to reduce dimensionality. We train the model using Adam [24] with a learning rate of 1e-3 until the training accuracy is greater than 99.99%, giving a validation accuracy

⁶ we use a threshold of 0.01 to help reduce the false discovery rate

Table 1: The number of each channels for the models trained on the simple, standard and spatial versions of the Elements dataset.

Layer	Model		
	Simple	Standard	Spatial
layers.0	64	64	64
layers.1	64	64	64
layers.2	64	64	128
layers.3	64	128	256
layers.4	64	128	256
layers.5	64	128	256

of 99.98% for the standard dataset. We use a different number of channels for the models trained on different datasets. This allows us to provide more model capacity when needed. The number of channels per layer for each model/dataset is summarised in Table 1.

The models for datasets \mathbb{E}_2 and \mathbb{E}_3 in Sec. 6.2 are the same architecture as for the simple dataset (\mathbb{E}_1).

Probe Dataset For Elements, the probe datasets are generated so that the positive examples for a concept contain only objects with that concept, so, for example, a red concept image will contain four objects with random shapes and textures that occur within the dataset, but all of them will be red. The negative set consists of random samples from the dataset.

11.3 ImageNet

ImageNet is used to demonstrate the experiments on a real-world application.

Classification Model We use the default weights for a ResNet-50 [20] in the TorchVision package in PyTorch, which used a variety of data augmentation techniques including Mixup [47], Cutmix [46], TrivialAugment [31], and Batch Augmentation [21].

Probe Dataset Most probe datasets used to train CAVs were collated from the Broden dataset [5], particularly focusing on textures such as **striped**, **meshed** or **dotted**, or objects such as **car**, **sea** or **person**. Some concepts were manually curated, such as the **anemone** concept, which was collected from test images of the ‘anemone fish’ class from ImageNet that were not used elsewhere in the experiments. Examples of some of these concepts are available in Figure 7.

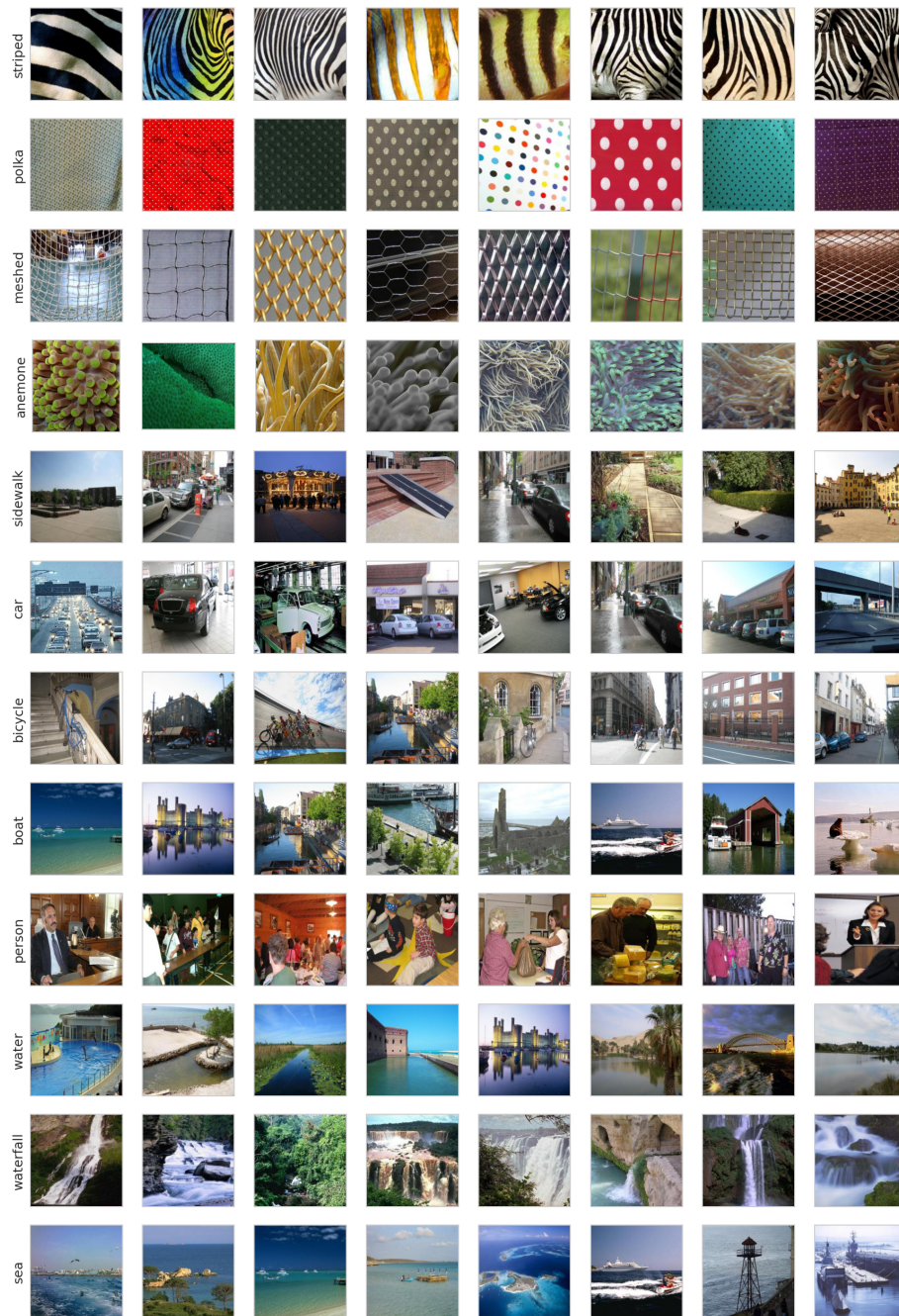


Fig. 7: Example positive probe datasets for different concepts for ImageNet.

11.4 Layer Selection

When creating CAVs, we need to choose a model layer. For the small CNN used for Elements, we can create CAVs for all layers, but for larger models, such as the ResNet-50 for ImageNet, it is computationally infeasible. In this paper, we focus on layers near the end of the model. The justification for this is twofold. (1) From an information theory perspective, the activations earlier in the network may contain more irrelevant information, suggesting the activations closer to the output may be more relevant to the prediction [29, 41]. We aim to use TCAV to explain the model output, therefore later layers may be more desirable. (2) The model representations may be more complex in later layers. This allows us to create CAVs for more complex concepts. We find that the empirical evidence supports these hypotheses. Figures 8 and 9 show the accuracy of the linear classifiers used to create the CAVs on a held-out test set for each probe dataset. The accuracy for each concept tends to increase in later layers. This suggests the CAVs better capture the model representations in later layers. However, we observe variation across the concepts. For example, the colours in Elements are easily classified in all layers, whereas the shapes/textures have lower performance in layers.1. As our goal is to understand the behaviour of concept vectors (when the concept is represented), we focus on CAVs that obtain at least 90% test accuracy. Therefore, we omit layers.1 in our analysis.

We do not create CAVs for the final convolutional layer in either the simple CNNs for Elements (layers.5) or the ResNet-50 for ImageNet (layer4.2) due to the gradient behaviour in these layers. In both cases, the network has no non-linearities after the layer. Therefore, the gradient of the logit with respect to the activations solely depends on the model weights, not the activations. TCAV relies on having a distribution of directional derivatives, which are then thresholded and averaged over different data points. For these layers, the gradient is the same for all inputs, and hence so is the directional derivative. This means the TCAV score for an individual CAV in these layers will be exactly 1 or 0. As such, we do not perform TCAV on layers after which there are no non-linearities.

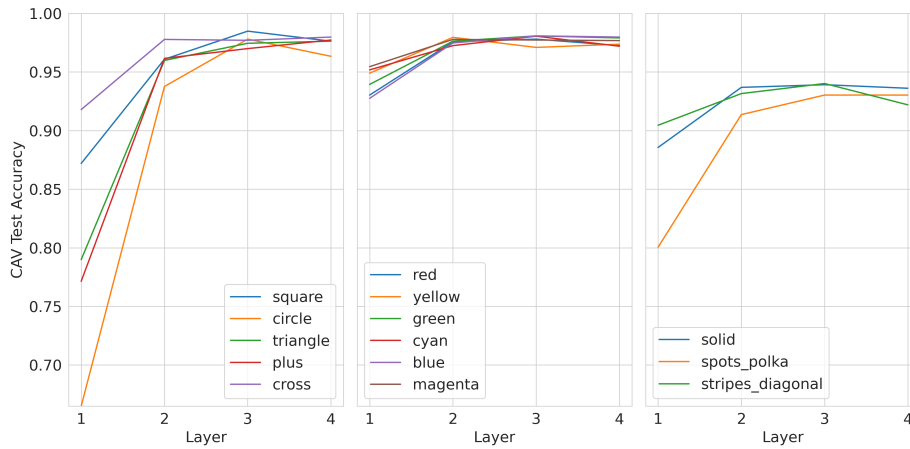


Fig. 8: Mean test accuracy for the linear classifiers from which the CAVs are generated for all concepts in the standard Elements dataset (split by concept type).

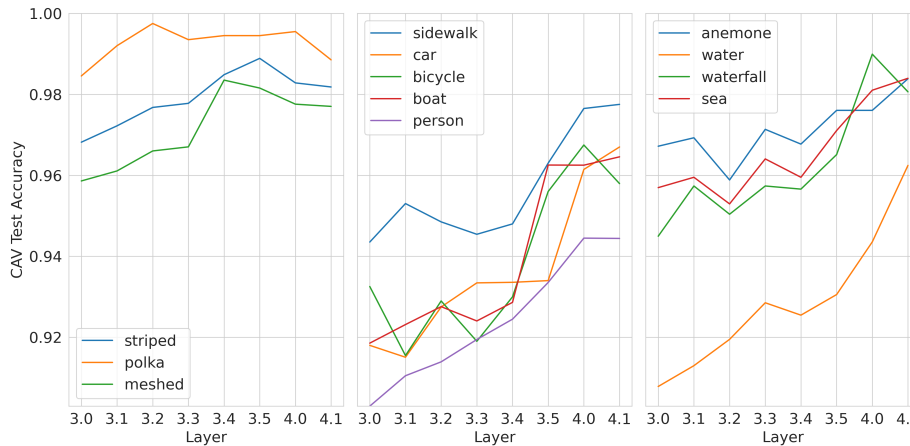


Fig. 9: Mean test accuracy for the linear classifiers from which the CAVs are generated for a selection of concepts in ImageNet.

12 Elements Dataset

12.1 Benefits of the Elements Dataset

Configurable datasets The configurable nature of the dataset allow us to explore different properties of the model and of CAVs. For example, we can introduce an association between the red and striped concepts in the training set by requiring

that all red elements are striped; or we can create a probe dataset of red elements on the right of the image to explore CAV spatial dependence.

Ground truth model behaviour The classes are configured as combinations of the elements’ shape, colour and texture. Therefore, by construction, we have the ground truth relationship between each concept and class. As these relationships are within the dataset, knowing the ground truth relationship between each concept and class does not allow us to explore model faithfulness. For that, we need the ground truth influence of each concept on model predictions. By having a class for each possible combination concepts, the model must learn linearly separable representations of the concepts in the representation space (before the final linear layer) of the NN to achieve a high accuracy. Therefore, we have the ground-truth relationship of how each concept influences the model’s predictions and can explore the faithfulness of concept-based explanation methods.

12.2 Elements Configuration

In the Elements dataset, there are various attributes we can vary. These attributes come in two types – image attributes and element attributes. The image attributes are: the number of elements per image and the size of the image. The element attributes are: colour, brightness, size, shape, texture, texture shift, and x and y coordinates within the image. Most are self-explanatory from their name, but texture shift requires more explanation. It is a small change in how the texture is applied to the object so that, for example, spots are not always in the same location with respect to the edge of the object. In this section, we describe the values that each of these attributes can take for the different versions of Elements that are used in the paper.

Standard The default version contains four objects in each image and the allowed concepts are the primary colours and their pairwise combinations (red, green, blue, yellow, cyan, magenta), five shapes (square, circle, triangle, plus, cross) and three textures (solid, spots and diagonal stripes).

Simple In some experiments, when stated, we use a simpler version which contains fewer shapes and colours. This is to reduce the complexity of the figures. The standard and simple dataset configurations are in Table 2.

Spatially Dependent For some experiments in Sec. 6.3 we use a spatially dependent version of the standard Elements dataset. This has the same configuration but introduces spatially dependent classes. As in the standard dataset, there is a class for all combinations of two and three concepts, *e.g.* ‘striped squares’ or ‘spotted cyan triangles’. However, there are additional classes which depend on where the element is present in the image. For all classes involving triangles, we add two new classes which depend on if the object is in the top or bottom half of the image. For example, the class ‘blue triangles’ will now have two additional

classes related to it of ‘blue triangles on the top’ and ‘blue triangles on the bottom’. Similarly, we introduce two new classes for all classes involving squares, but for the left/right halves of the image rather than the top/bottom.

Entangled We use two alternative versions of the simple dataset in the Entanglement experiments: \mathbb{E}_2 and \mathbb{E}_3 . As described in the main text, these are identical to the simple dataset, apart from the association between the red and triangle concepts. In each case, we restrict some of the allowed combinations of concepts that an element can take. This also removes some classes from the dataset which we reflect in any trained models. \mathbb{E}_2 does not allow any shape apart from triangles to be red. This removes classes like ‘red circles’ or ‘spotted red squares’. \mathbb{E}_3 has this restriction and then places a further restriction that triangles have to red. This removes classes such as ‘blue triangles’ or ‘striped green triangles’.

Table 2: The configurations for the standard and simple versions of the elements dataset. Element size and image size are in pixels. Brightness is the value of the pixels in the element.

Property	Dataset	
	Standard	Simple
Colours	red, green, blue, yellow, cyan, magenta	red, green, blue
Shapes	square, circle, triangle, plus, cross	square, circle, triangle, plus
Textures	spots, stripes	spots, stripes
Brightness	153-255	153-255
Element Size / pixels	48-80	48-80
No. Elements per image	4	4
Image Size / pixels	256	256

12.3 Examples

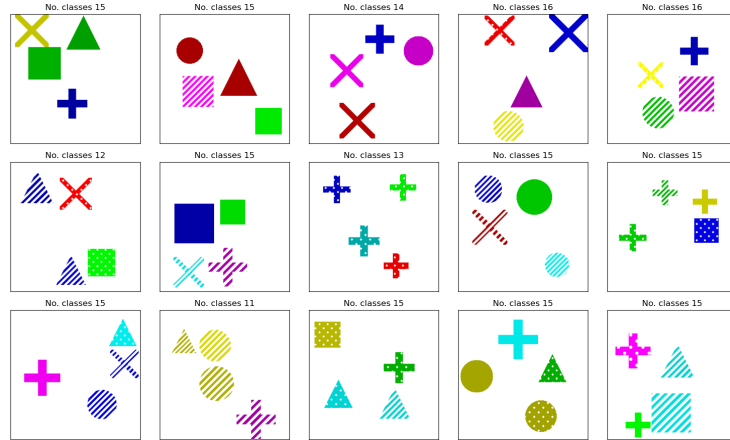


Fig. 10: Example images from the standard elements dataset. The number of classes each image belongs to is displayed above it.

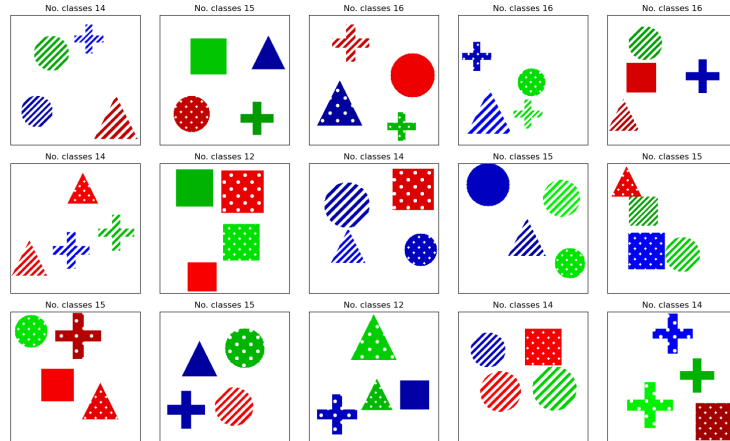


Fig. 11: Example images from the simple elements dataset. The number of classes each image belongs to is displayed above it.

13 Consistency Experiment Details

Figure 3 shows the consistency error for various types of CAV. In this section, we describe how we find the different types of CAV. In each case, v_{c,l_1} is a CAV

trained as normal using a probe dataset, whereas the creation method for \mathbf{v}_{c,l_2} varies for each experiment and is described below:

Optimised CAV We use gradient descent to optimise \mathbf{v}_{c,l_2} to minimise the consistency error:

$$\arg \min_{\mathbf{v}_{c,l_2}} \|f(\mathbf{a}_{l_1} + \mathbf{v}_{c,l_1}) - (\mathbf{a}_{l_2} + \mathbf{v}_{c,l_2})\| \quad (30)$$

The starting point for each optimisation process is a CAV in layer l_2 , $\mathbf{v}_{c,l_2}^{r_2}$, trained on a different random probe dataset. The nearly identical errors for each optimisation process support the likelihood of a global minimum being reached.

Concept CAV These are simply normal CAVs trained as described in Sections 2 and 11, *i.e.*, the CAVs are trained using a probe dataset containing \mathbb{X}_c^+ and \mathbb{X}_c^- . The distribution is over r_2 for different random probe datasets \mathbb{X}_{c,r_2} for \mathbf{v}_{c,l_2} , where $r_2 \neq r_1$ denotes the random set.

Projected CAV CAVs in layer l_1 projected into layer l_2 using f : $f(\mathbf{v}_{c,l_1})$. The distribution is over different CAVs in layer l_1 , *i.e.* \mathbf{v}_{c,l_1}^r .

Random CAV CAVs trained using a random probe dataset for both the positive and negative sets:

$$\begin{aligned} \mathbb{X}_c^- &= \mathbb{X}_{c,r_1}^- \\ \mathbb{X}_c^+ &= \mathbb{X}_{c,r_2}^-, \quad r_2 \neq r_1 \end{aligned} \quad (31)$$

Random Direction Each element of \mathbf{v}_{c,l_2} is drawn from a uniform distribution between $[-0.5, 0.5]$, and rescaled to be a unit vector. The distribution is over different random seeds for the random number generator.

13.1 Scaling perturbations

To ensure that $\mathbf{a}_l + \mathbf{v}_{c,l}$ stays in-distribution, we scale the perturbations as follows:

$$\hat{\mathbf{a}}_l = \mathbf{a}_l + \gamma \mathbf{v}_{c,l} \frac{\overline{\|\mathbf{a}_l\|}}{\|\mathbf{v}_{c,l}\|}, \quad (32)$$

where γ is a hyperparameter used for perturbation size (typically set to 0.01), $\|\cdot\|$ the L_2 norm of a vector, and $\overline{\|\mathbf{a}_l\|}$ the average norm of \mathbf{a}_l . We scale the perturbation by the mean activation norm to account for the difference in the norms between the activation and concept vector to have consistently sized perturbations across layers.

We performed experiments to explore the sensitivity of consistency error to the size of the perturbation, γ , for various layers and concepts for the ImageNet and Elements datasets. In Figures 12 and 13, we show the results for a variety of concepts for both the ImageNet and Elements datasets. Similar patterns were observed across experiments. As we increase $|\gamma|$, the consistency error scales linearly, as a larger perturbation causes a larger difference between $f(\hat{\mathbf{a}}_{l_1})$ and $\hat{\mathbf{a}}_{l_2}$. The scale of the y axis on the left of Figures 12 and 13 is not particularly

meaningful without context, so we scale it by the norm of the perturbation in layer l_2 , $\|\gamma \mathbf{v}_{c,l_2} \frac{\|\mathbf{a}_{l_2}\|}{\|\mathbf{v}_{c,l_2}\|}\|$, on the right of the same figures. Values greater than one mean that the difference between $f(\hat{\mathbf{a}}_{l_1})$ and $\hat{\mathbf{a}}_{l_2}$ are larger than the perturbation made in layer l_2 .

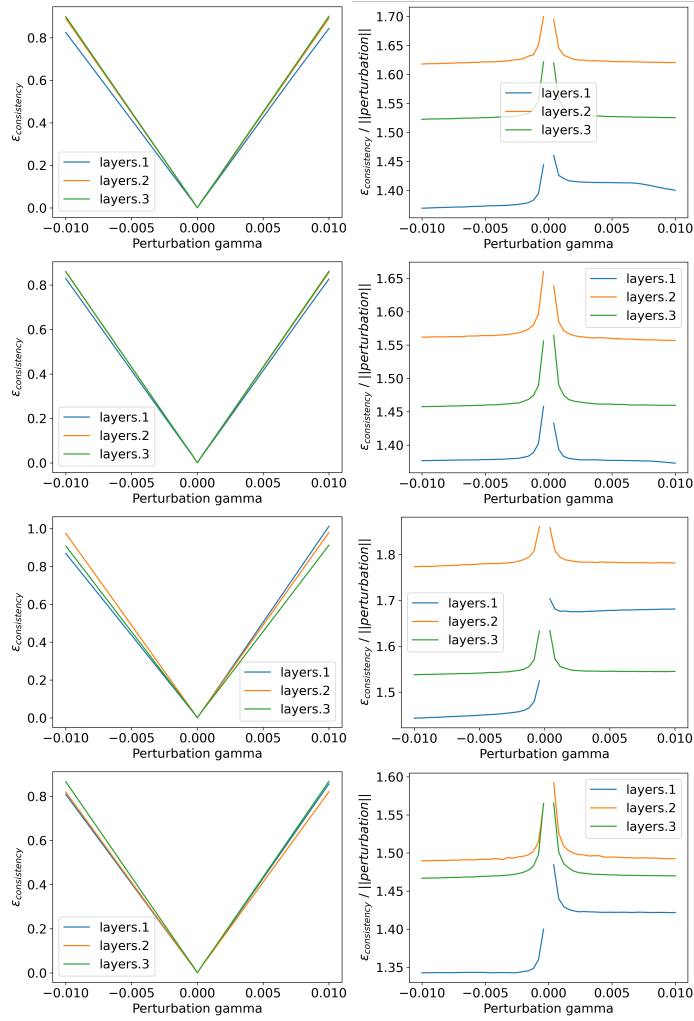


Fig. 12: The mean consistency error for (from top to bottom) red, blue, triangle and striped CAVs across layers (left) scaled by the size of the perturbation (right) for the Elements dataset.

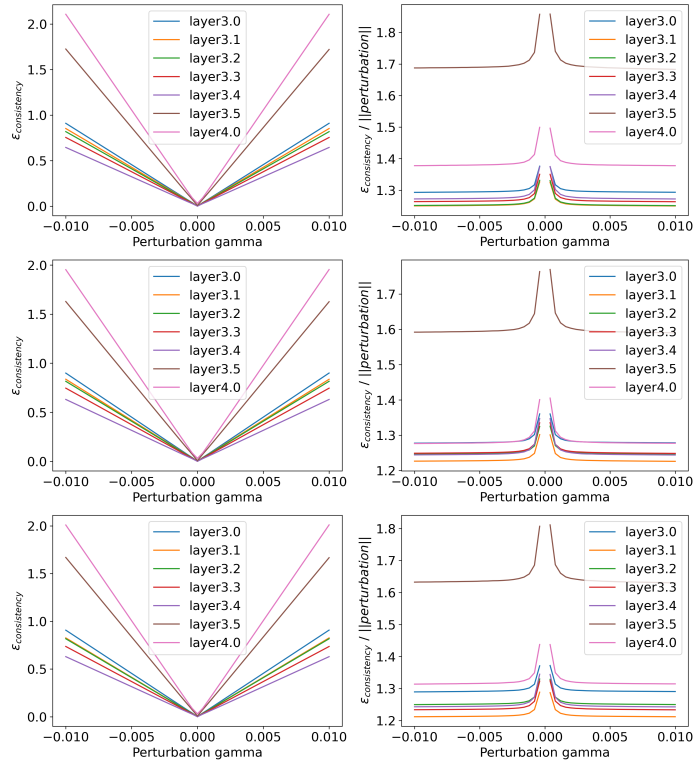


Fig. 13: The mean consistency error across 10 CAVs for **striped** (top), **lined** (middle) and **dotted** (bottom) CAVs across layers (left) scaled by the size of the perturbation (right) for a ResNet-50 train on ImageNet.

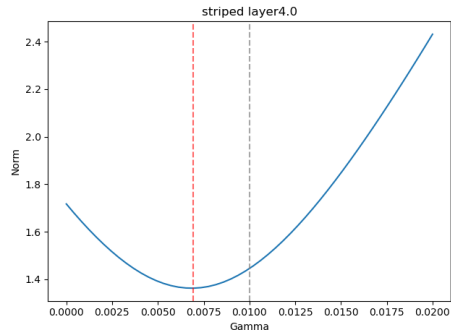


Fig. 14: The sensitivity of the mean consistency error to scaling γ for an optimised CAV for the penultimate convolutional layer in a ResNet50 trained on ImageNet.

13.2 Additional results

In this section we provide additional results for the different consistency experiments as in Fig. 3. We include the results for multiple concepts and layers for both the ImageNet and Elements datasets. To allow for better comparison between layers, we normalise the consistency errors in some of the figures. For each layer, the consistency error is divided by the mean error for the optimised CAVs. For the normalised plots, a value of one can be seen as the lowest error possible for that layer. The relative ordering of layers is approximately consistent across the different types of CAV. For example, in Fig. 15, there is a downward trend between layer3.0 to layer3.5 and then an increase for layer4.0.

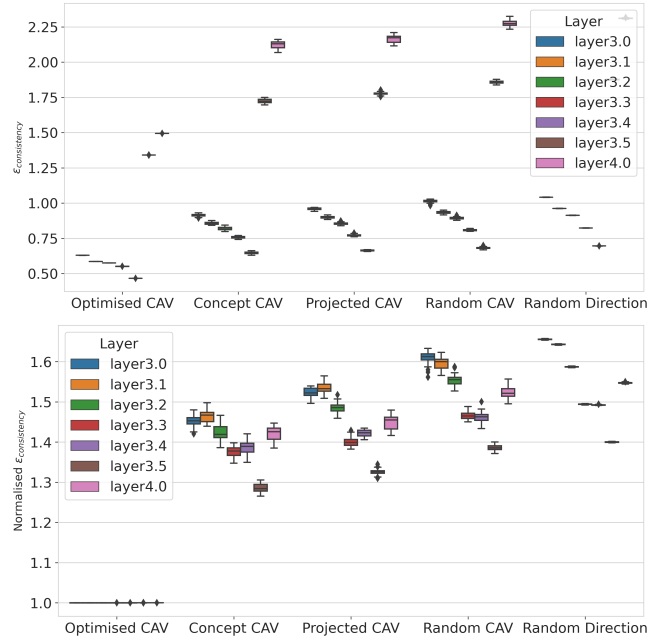


Fig. 15: The distribution of consistency errors (top) and normalised consistency errors (bottom) for different \mathbf{v}_{c,l_2} for **striped** in a selection of layers from a ResNet-50 trained on ImageNet. Optimised CAV: The lower bound – a vector optimised to have the minimum error. Concept CAV: **striped** CAVs, trained as normal. Projected CAV: **striped** CAVs from layer l_1 projected into layer l_2 , $f(\mathbf{v}_{c,l_1})$. Random CAV: CAVs with random images for the probe dataset. Random Direction: Random vectors drawn from a uniform distribution.

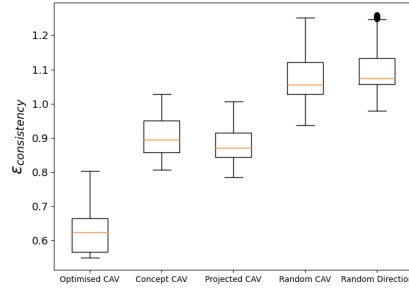


Fig. 16: The distribution of consistency errors for different \mathbf{v}_{c,l_2} for **square**, **triangle**, **red**, **green**, **solid** and **stripes** CAVs for ‘layers.1’, ‘layers.2’ and ‘layers.3’ of a CNN trained on the Elements dataset. Optimised CAV: The lower bound – a vector optimised to have the minimum error. Concept CAV: CAVs, trained as normal. Projected CAV: striped CAVs from layer l_1 projected into layer l_2 , $f(\mathbf{v}_{c,l_1})$. Random CAV: CAVs with random images for the probe dataset. Random Direction: Random vectors drawn from a uniform distribution.

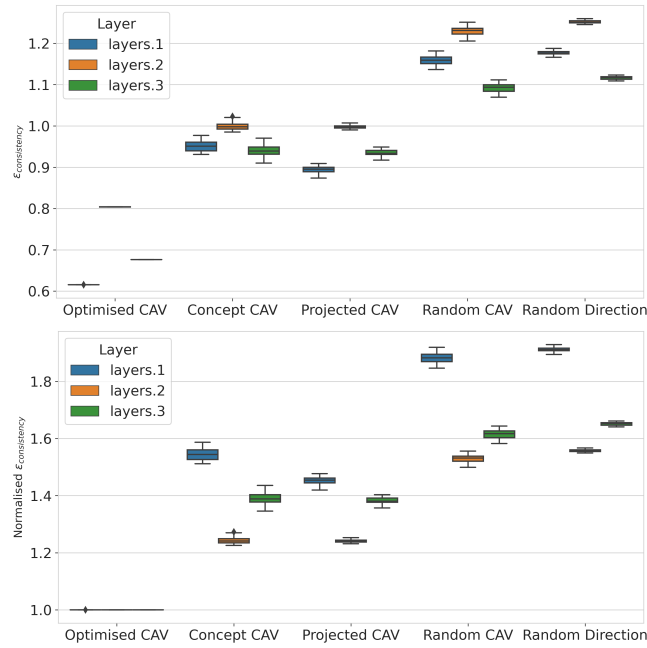


Fig. 17: The distribution of consistency errors (top) and normalised consistency errors (bottom) for different \mathbf{v}_{c,l_2} for **square** CAVs for a variety of layers for the Elements dataset. Optimised CAV: The lower bound – a vector optimised to have the minimum error. Concept CAV: CAVs, trained as normal. Projected CAV: striped CAVs from layer l_1 projected into layer l_2 , $f(\mathbf{v}_{c,l_1})$. Random CAV: CAVs with random images for the probe dataset. Random Direction: Random vectors drawn from a uniform distribution.

13.3 DeepDream

DeepDream [30] is a feature visualisation tool. It starts from an image, generated by sampling noise from a random uniform distribution and then iteratively updates the input image to maximise the L2 norm of activations of a particular layer. We use a similar approach but instead maximise the dot product between the activations and a CAV: $\mathbf{v}_{c,l} \cdot \mathbf{a}_l$. In Figures 18 and 19, we show these visualisations for a selection of ImageNet CAVs for successive layers in a ResNet-50.

These visualisations offer qualitative evidence that the CAVs represent different components of the same concept in different layers. For example, the **car** concept in Figure 18 consists of many square box-like objects in earlier layers, but nothing recognisable as a car, whereas, in later layers, whole car sections can be seen in the visualisations.

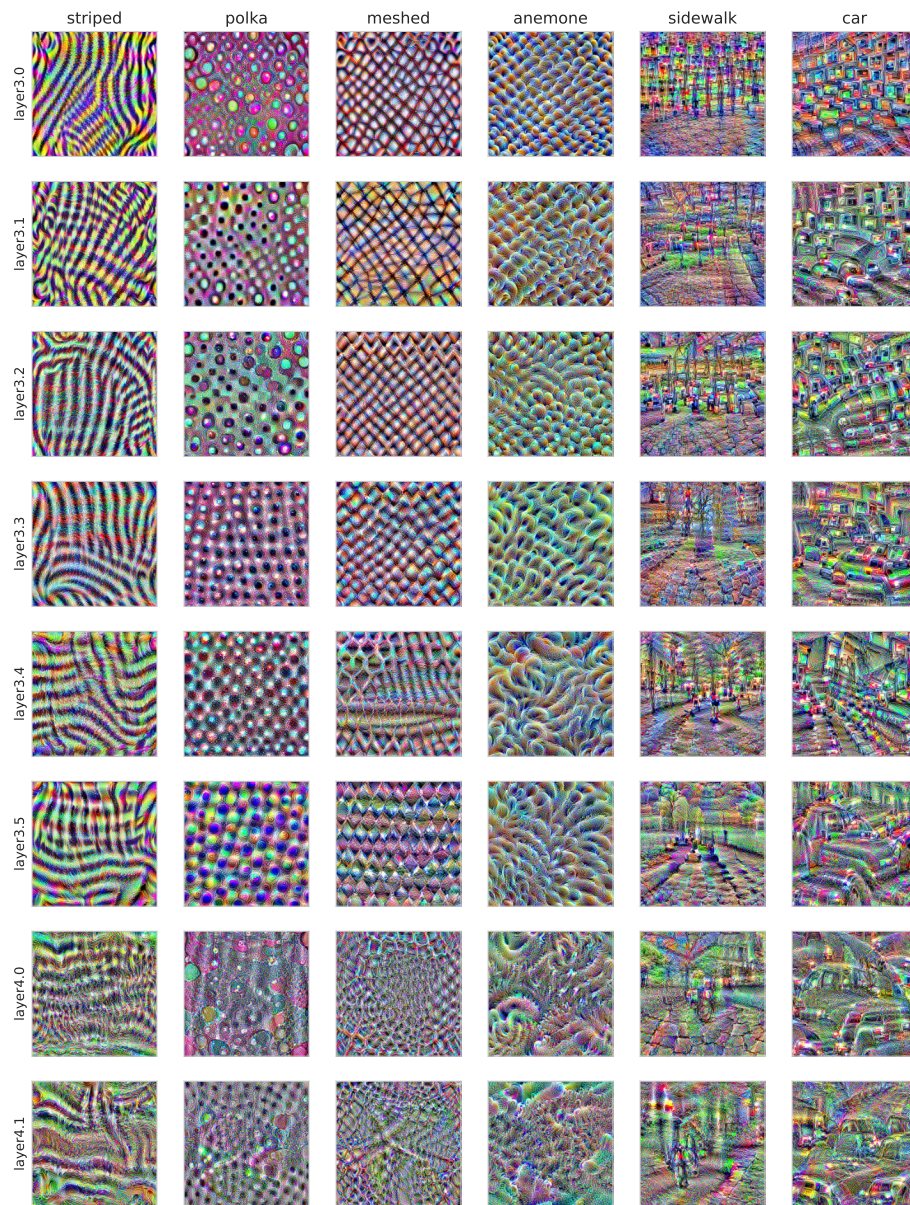


Fig. 18: CAV visualisations using DeepDream for a selection of concepts from ImageNet. Each row corresponds to a layer of a ResNet-50 and each column a different concept.

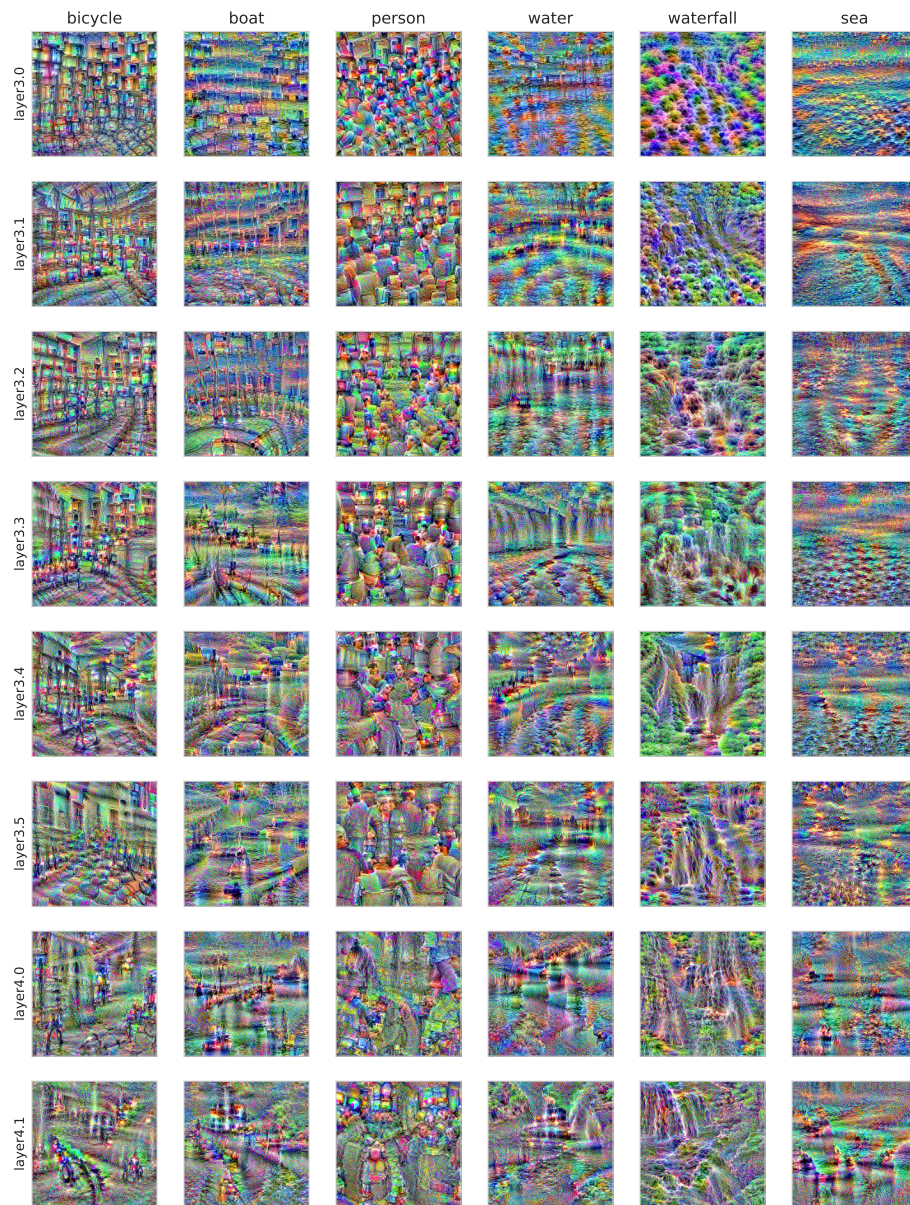
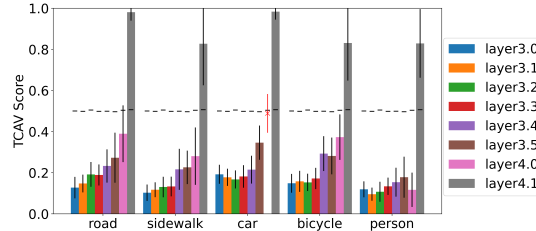


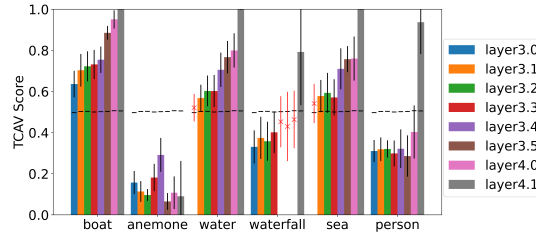
Fig. 19: CAV visualisations using DeepDream for a selection of concepts from ImageNet. Each row corresponds to a layer of a ResNet-50 and each column a different concept.

13.4 Inconsistent TCAV Scores

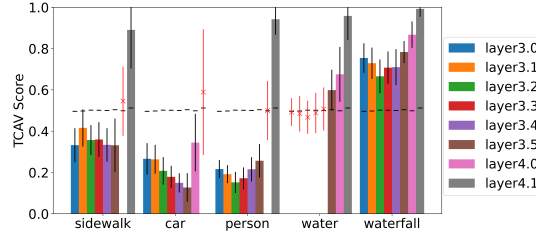
In this section, we display additional examples of inconsistent TCAV scores across layers for ImageNet classes. In Figure 20 each subfigure contains at least one concept that has inconsistent TCAV scores. We include example images from those classes in Fig. 21.



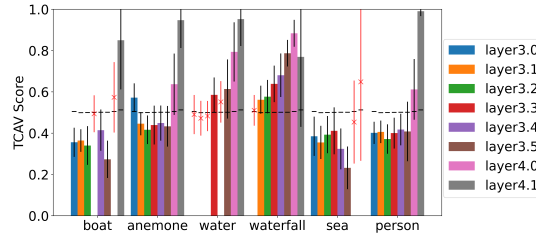
(a) TCAV scores for a selection of concepts for the ‘car wheel’ class in ImageNet.



(b) TCAV scores for a selection of concepts for the ‘dock’ class in ImageNet.



(c) TCAV scores for a selection of concepts for the ‘sidewalk’ class in ImageNet.



(d) TCAV scores for a selection of concepts for the ‘lionfish’ class in ImageNet.

Fig. 20: Inconsistent TCAV scores for a selection of concepts and classes in ImageNet. The standard deviation is shown in black for significant results and red for insignificant results. The mean TCAV score for random CAVs are shown as horizontal black lines.

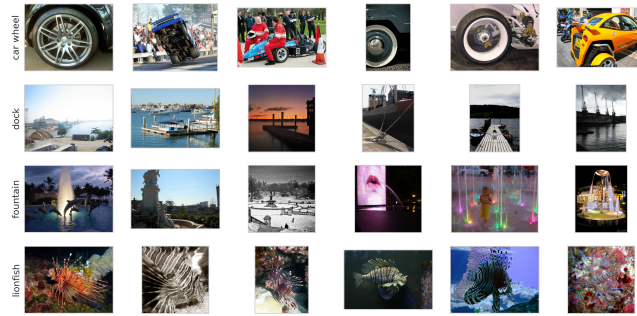


Fig. 21: Example images from a selection of ImageNet classes.

14 Entanglement Experiment Details

We use cosine distance to measure how similar two CAVs are. Assuming the CAVs, $v_{c_1,l}$ and $v_{c_2,l}$, are unit vectors this simplifies to the dot product of the two:

$$\begin{aligned} \text{Cosine Similarity} &= \frac{\mathbf{v}_{c_1,l} \cdot \mathbf{v}_{c_2,l}}{\|\mathbf{v}_{c_1,l}\| + \|\mathbf{v}_{c_2,l}\|} \\ &= \mathbf{v}_{c_1,l} \cdot \mathbf{v}_{c_2,l} \end{aligned} \quad (33)$$

In our visualisations (Fig. 4 and Sec. 14.1) we compare multiple CAVs for each concept, each with a different random probe dataset, denoted by r . This allows us to see how similar CAVs for the same concept are on repeat training runs. Each value in the visualisation is the mean cosine similarity between the concepts on its corresponding x and y axis labels between all CAVs which do not have the same random probe dataset, i.e.:

$$\sum_{r_1}^R \sum_{r_2 \neq r_1}^R \frac{\mathbf{v}_{c_1,l}^{r_1} \cdot \mathbf{v}_{c_2,l}^{r_2}}{R(R-1)} \quad (34)$$

where $\mathbf{v}_{c_1,l}^{r_1}$ is the CAV corresponding to concept c_1 , layer l and random probe dataset \mathbb{X}_{c,r_1} .

14.1 Additional Results

Elements In Fig. 22, we show the cosine similarities for all concepts in the standard Elements dataset. The conclusions are similar to the visualisation for \mathbb{E}_1 in Fig. 4, but the negative associations between the mutually exclusive concepts are weaker. We hypothesise that this is because there are more concepts within each group. This is empirically justified as the average cosine similarity of each group approximately corresponds to the number of concepts in the group. If this hypothesis is true, it makes it unlikely that we will find similar groupings in real

datasets containing natural images as concepts are rarely partitioned as neatly or in as few possible combinations.

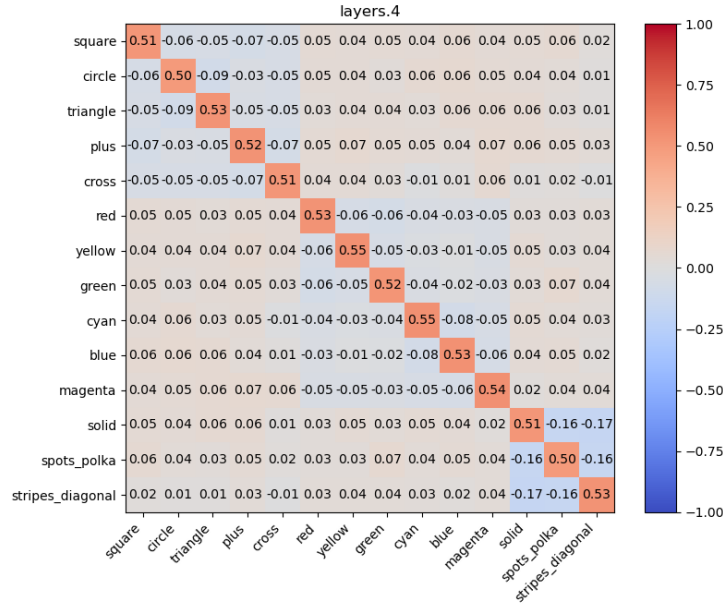


Fig. 22: Mean pairwise cosine similarities between 30 CAVs for different concepts from the standard Element dataset.

ImageNet In Figure 23, we show the pairwise cosine similarities for a selection of concepts for a ResNet-50 trained on ImageNet. The associations between concepts are less clear-cut than for Elements, but qualitatively they make intuitive sense. For example, the concepts most similar to **field** are **grass** and **earth**, in the top of Figure 23, and the concepts most similar to **sidewalk** are **bicycle**, **road** and **hedge**. The latter makes sense as many of the **hedge** exemplars in the probe dataset are next to a path or road. This emphasises the importance of designing your probe dataset to match the concept you want the CAV to represent.

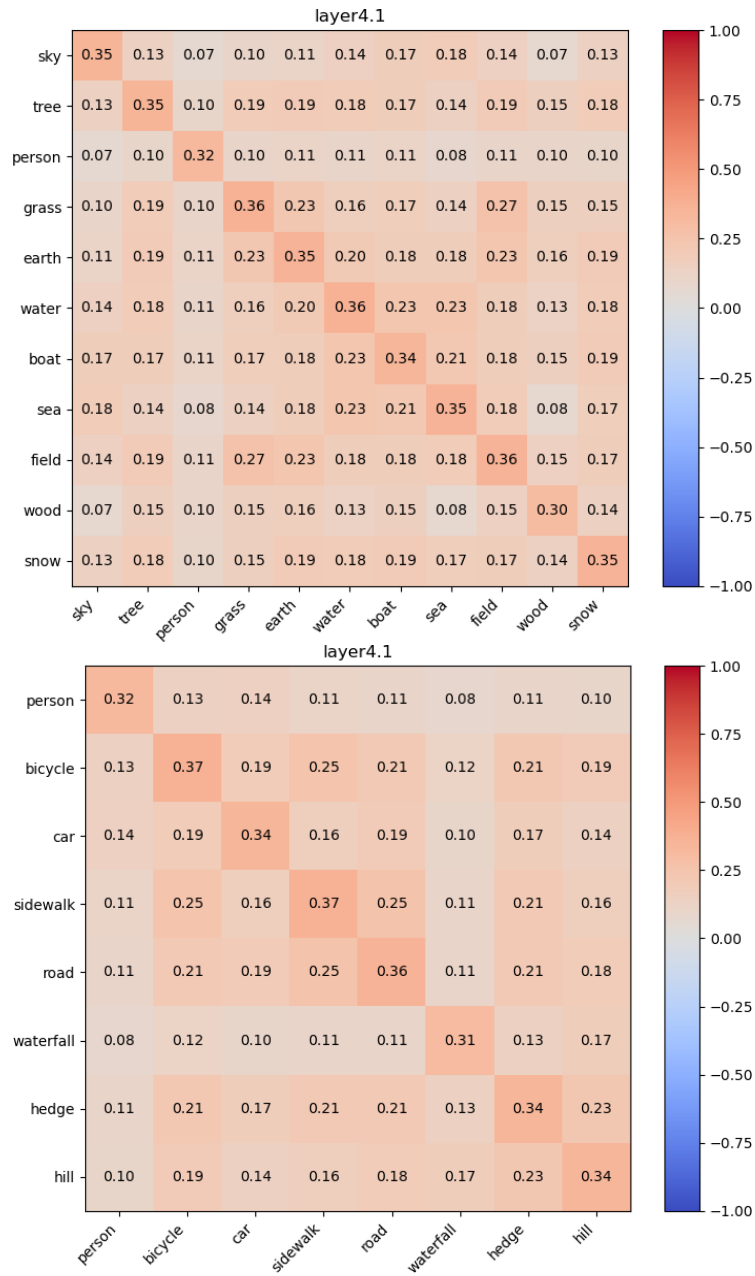


Fig. 23: Mean pairwise cosine similarities between 30 CAVs for different concepts from ImageNet.

14.2 Polysemanticity

In Figures 4 and 22 we find that the vector representations of mutually exclusive concepts are anti-correlated with each other. Each concept vector does not just mean, for example, **red**. It means **red**, **not green** and **not blue**.

Elhage *et al.* [13] also find evidence for polysemantic representations. However, they found individual neurons which were polysemantic, whereas here vectors, i.e., groups of neurons, are polysemantic. In addition, the reasoning is different. The polysemanticity discussed in Elhage *et al.* [13] is caused by sparse features being compressed into fewer neurons than there are features. Here, we do not have sparse features and have more neurons than features. Instead, the polysemanticity is caused by associations between the concepts and the optimisation process favouring negatively correlated representations for mutually exclusive concepts.

14.3 Dot product distributions

The definition of entangled concepts in Eq. (6) uses the dot products of a CAV trained on concept c_1 with the the activations of a probe dataset for a different concept c_2 . Figure Fig. 24 shows the distribution of dot products for a selection of CAVs, model training datasets and concept probe datasets. We use the same set of Elements datasets as in Sec. 6.2: \mathbb{E}_1 , \mathbb{E}_2 , \mathbb{E}_3 , where \mathbb{E}_1 has no association between **red** and **triangle** and \mathbb{E}_2 and \mathbb{E}_3 have successively stronger associations between the concepts. This changing association is apparent in the dot product distributions. For \mathbb{E}_1 , the dot products of the test probe datasets differing from the CAV concept do not differ significantly from the dot products for random images (the negative probe dataset). Whereas, for \mathbb{E}_2 and \mathbb{E}_3 , the random distribution is shifted lower than for either CAV, even if the CAV is labelled differently from the test dataset. This shows that the **red** and **triangle** CAVs are entangled for these datasets/models.

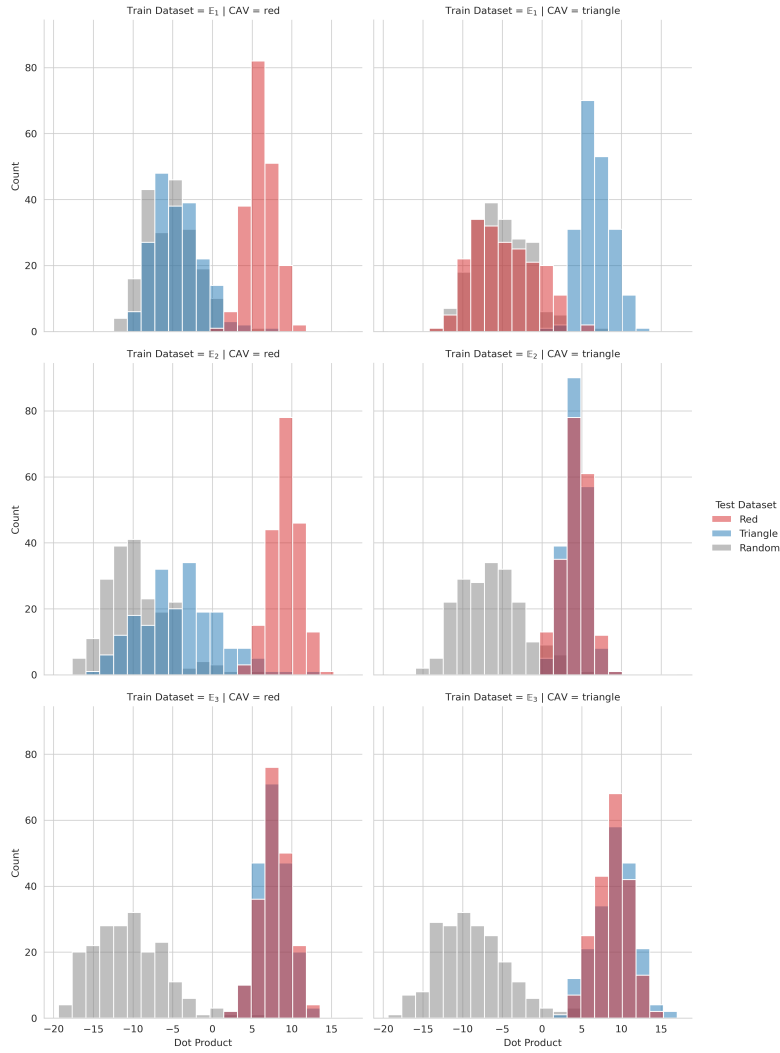


Fig. 24: Distribution of dot products ($v_{c_1,l} \cdot a_{c_2,l}$) for the three versions of Elements with increasing association between **red** and **triangle** (E_1 , E_2 and E_3). The distribution of dot products are displayed for three different test sets containing in-distribution images for **red**, **triangle** and **random** images.

15 Spatial Dependency Experiment Details

15.1 Spatially Dependent Probe Datasets

For Elements, the probe datasets contained elements that only appear in specified locations – an example is shown in Fig. 2. For ImageNet, we do not have

direct control of where objects can appear. Therefore, we greyed out different regions of the image. For example, we created oppositely dependent concepts by either greying out the middle of the image, or the edges - see Appendix 15.1 for examples.

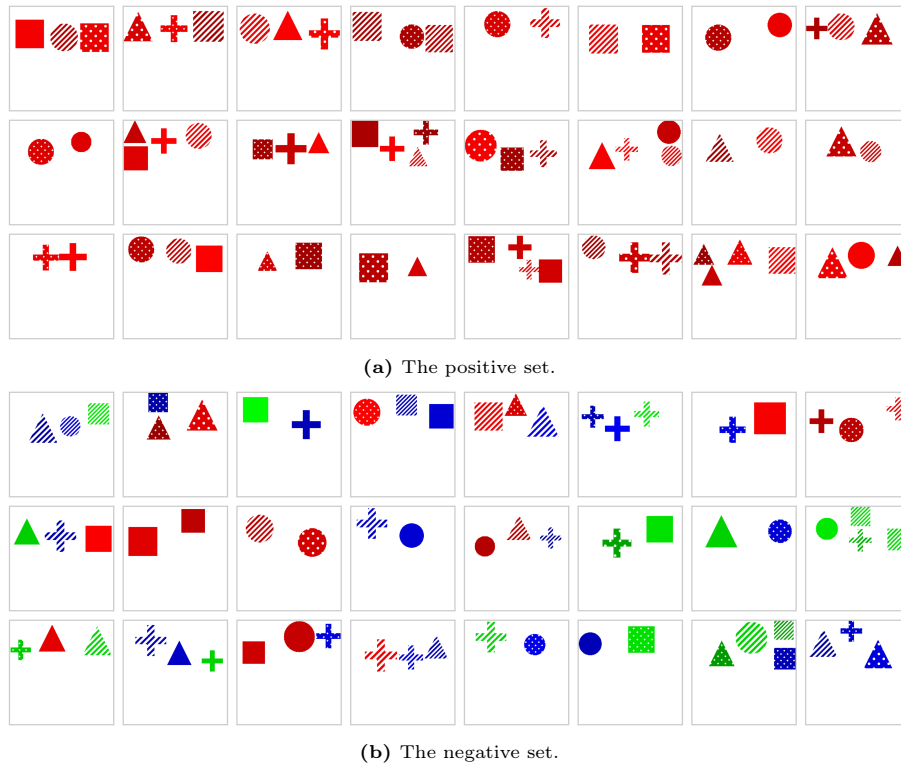
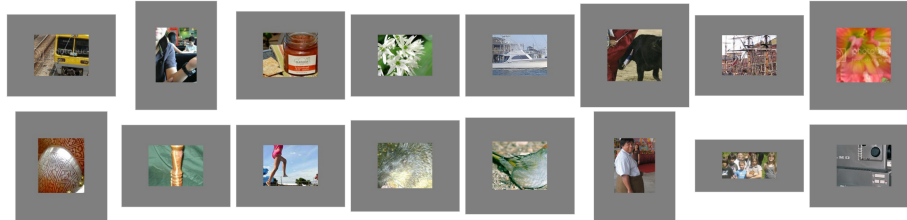


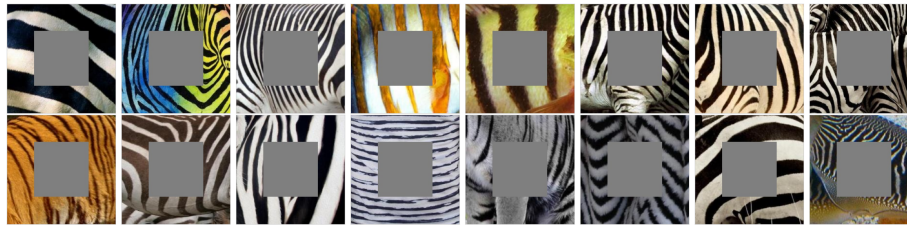
Fig. 25: Example images for the positive and negative sets of the probe dataset for the red top in the simple elements dataset.



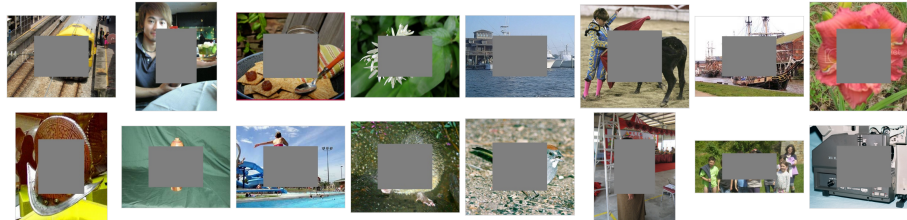
(a) The positive set for striped middle.



(b) The negative set for striped middle concept.



(c) The positive set for striped edges concept.



(d) The negative set for striped edges.

Fig. 26: Example images from spatially dependent probe datasets for ImageNet.

15.2 Spatial Norms Details

When finding CAVs, we use the activations of layer l in a convolutional neural network, which has shape $H \times W \times D$, where H , W and D are the height, width and number of channels, respectively. When finding the CAV, these activations are flattened to be vectors of length $m = H \times W \times D$. The value of each element in the activations depends on its specific height, width and depth indices. As a result, each corresponding element of the resultant CAV is also index-dependent. We are interested in spatial dependence, so to visualise how a CAV varies across

the width and depth dimensions we calculate the L2 norm of each depth-wise slice – the CAV’s spatial norms.

15.3 Individual Spatial Norms

In Fig. 27, we present the spatial norms for `striped` in a ResNet trained on the ImageNet dataset. Each heatmap is for a different random probe dataset, denoted by r . The different patterns in the heatmaps show that each individual $\mathbf{v}_{c,l}^r$ has a spatial dependency which differs across r . However, when we average the norms across multiple CAVs, $\sum_{r=1}^R \mathbf{S}_{c,l}^r / R$, we obtain a uniform distribution across the spatial dimensions. This uniformity suggests that the spatial dependencies of each individual CAV cancel out across multiple seeds, as depicted in the top rows of Fig. 6 in the main text.

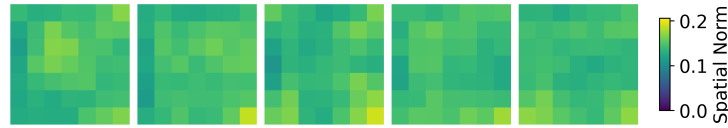


Fig. 27: Individual spatial norms for `striped`, where each CAV was trained on a different negative probe set, for layer4.1 of a ResNet trained on ImageNet.

15.4 Additional Spatial Norms

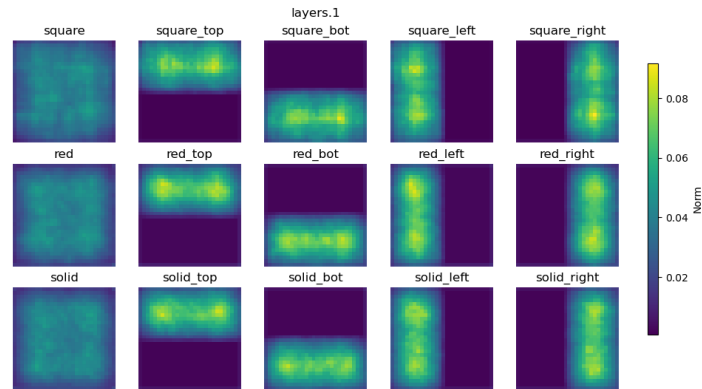


Fig. 28: Mean CAV spatial norms across 30 CAVs for a selection of concepts in the Element dataset for the second convolutional layer.

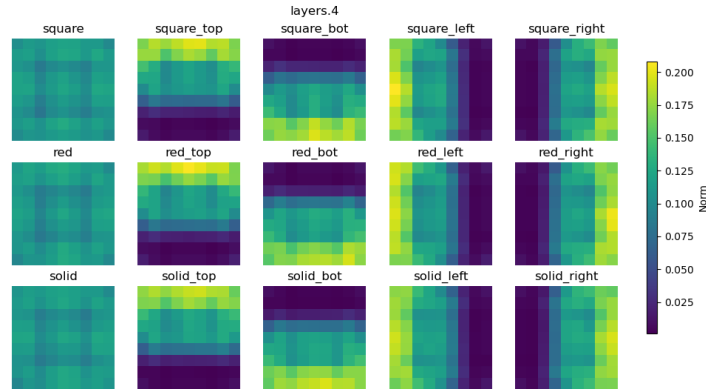


Fig. 29: Mean CAV spatial norms across 30 CAVs for a selection of concepts in the Element dataset for the fifth convolutional layer.

15.5 Spatial Means

Instead of visualising the norm of each depth-wise slice, we can visualise the mean. We default to showing the norm because you could have a spatial mean of zero in a region of activation space which has a large effect on the directional derivative. This could occur, for example, if half the elements of the CAV are large and positive and the corresponding gradients are positive, and half the elements of the CAV are large and negative and the corresponding gradients are also negative. This would lead to that spatial region having a large contribution to the directional derivative, but the spatial mean would be close to zero. The spatial norm, however, would be large for this region. This makes the norm a better measure of the effect of each region, but the mean can still be useful to show the direction of that effect.

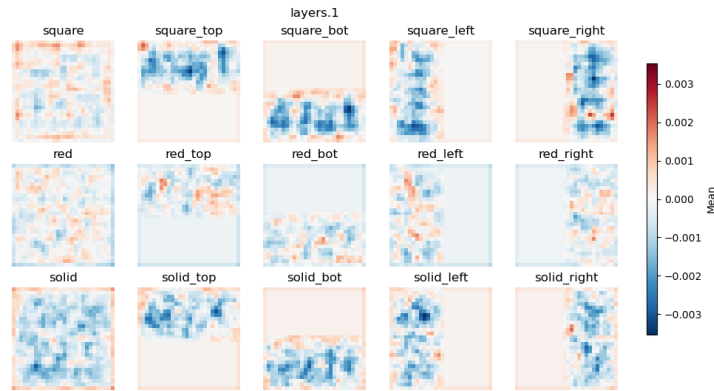


Fig. 30: Mean CAV spatial means across 30 CAVs for a selection of concepts in the Element dataset for the second convolutional layer.

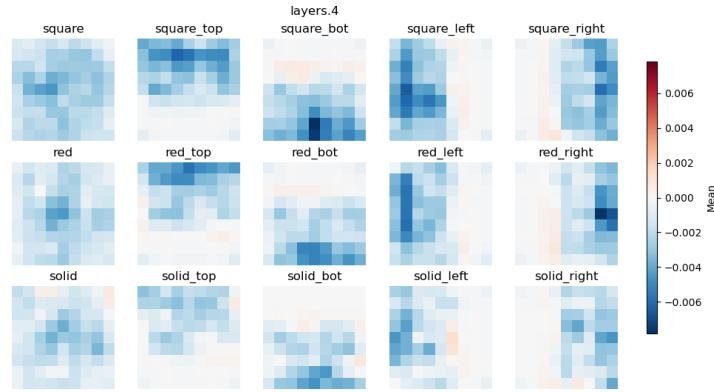
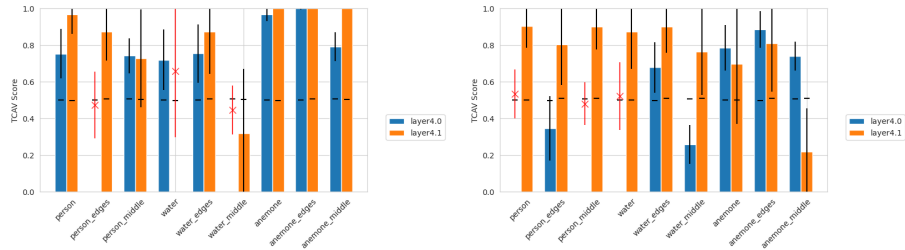


Fig. 31: Mean CAV spatial means across 30 CAVs for a selection of concepts in the Element dataset for the fifth convolutional layer.

15.6 Spatially Dependent TCAV Scores

In this section we provide example TCAV scores which differ across complementary spatially dependent CAVs, *i.e.*, for at least one concept, the TCAV score is the opposite side of the null for the **edges** version of a concept compared to the middle version (or the **left/right** and **top/bottom** versions).



(a) TCAV scores for a selection of concepts for the ‘anemone fish’ class in ImageNet. (b) TCAV scores for a selection of concepts for the ‘spiny lobster’ class in ImageNet.

Fig. 32: Examples of spatially dependent TCAV scores in ImageNet. Each subfigure is a separate class. The standard deviation is shown in black for significant results and red for insignificant results. The mean TCAV score for random CAVs are shown as horizontal black lines.

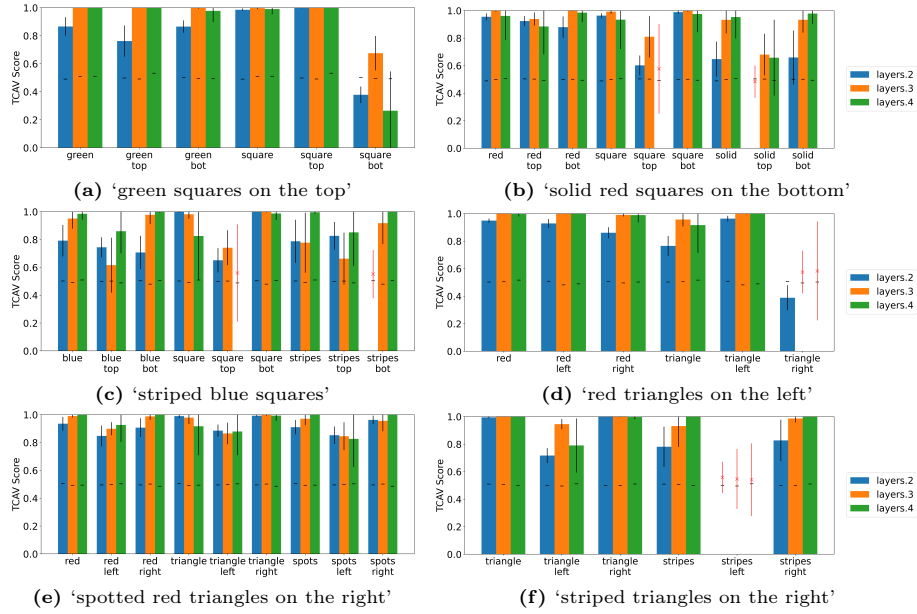


Fig. 33: Examples of spatially dependent TCAV scores in the spatially dependent version of Elements. Each subfigure is a separate class. The standard deviation is shown in black for significant results and red for insignificant results. The mean TCAV score for random CAVs are shown as horizontal black lines.

15.7 Dot product distributions

The definition of concept vector spatial dependence in Eq. (8) compares a CAV, $\mathbf{v}_{c,l}$, with the activations of two positive probe datasets with different spatial dependencies, \mathbf{a}_{c,l,μ_1}^+ and \mathbf{a}_{c,l,μ_2}^+ , by taking the dot product between them $\mathbf{a}_{c,l,\mu_x}^+ \cdot \mathbf{v}_{c,l}$. In Fig. 34, we show the distribution of dot products for three concepts and three test probe datasets in the spatially dependent version of Elements. The separation between the distributions for the `stripes left` and `stripes right` probe datasets (blue and green bars, respectively) for both the `stripes left` and `stripes right` CAVs (left and right plots, respectively) demonstrate that these CAVs are spatially dependent.

16 Further Related Work

Recent work highlighted problems with concept-based explanation methods. Ramaswamy *et al.* [34] showed that using different probe datasets to interpret the same model can lead to different explanations for the same concept. Similarly, Soni *et al.* [38] showed these methods to be sensitive to the random seed used to sample images for the negative set. Our work complements this research by

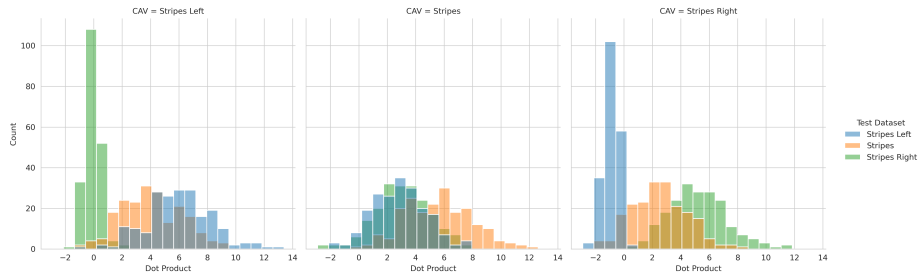


Fig. 34: Distribution of dot products between spatially dependent CAVs and image activations ($\mathbf{a}_{c,l,\mu}^+ \cdot \mathbf{v}_{c,l}$) for the spatially dependent Elements dataset. Each column is for different CAVs. From left to right these are: **stripes left**, **stripes**, **stripes right**. For each CAV we show the distribution for three positive probe datasets: **stripes left** (blue), **stripes** (orange), **stripes right** (green).

Table 3: Examples in computer vision and medical imaging research, where consistency, entanglement and spatial dependence may impact analyses. We use the following abbreviations: skin cancer (SC), skin lesions (SL), breast cancer (BC), histology (H) CIFAR-10/100 (CF) [25], COCO (CO) [27], CUB (CB) [40], Places365 (PI) [49], Waterbirds (Wb) [36], ImageNet (Im) [12]

Property	Medicine				CV Research					Papers	
	SC	SL	BC	H	CF	CO	CB	PI	Wb		Im
Consistency	✓	✓			✓	✓	✓	✓			[16, 18, 28, 34, 42, 45]
Entanglement	✓	✓	✓	✓	✓	✓	✓	✓	✓	✓	[16, 18, 19, 28, 33, 34, 42, 45]
Spatial Dependence	✓	✓	✓	✓	✓	✓	✓	✓	✓	✓	[16, 18, 28, 33, 34, 42, 45]

investigating the underlying properties of concept vectors and how they may cause problems when interpreting concept-based explanations.

Extensions to the original TCAV have been suggested, attempting to improve aspects of the original method. For instance, Ghorbani *et al.* [17] automate concept discovery by using super-pixels and clustering, removing the need to handcraft a probe dataset. Zhang *et al.* [48] and Schrouff *et al.* [37] change how CAVs are created to produce local and global explanations. However, these methods still use vectors to represent concepts [3]. As such, our work is still applicable to each of the extensions.

17 Example Use-case

In §7 we provided recommendations to better use CAVs in practice. To provide a concrete example, we next examine the use-case of Yan *et al.* [42] which uses CAVs in the context of skin cancer diagnosis. In the next few sections we will demonstrate with this concrete example three recommendations, and show how these recommendations could have impacted the conclusions drawn.

Consistency The authors use CAVs on a single layer. As discussed in § 6.1 and § 13, different layers can represent different aspects of the same concept. To have

a better understanding of the overall effect of the concept on the model, CAVs should be created for multiple layers.

Entanglement There are multiple concepts which have opposed meanings, for example **regular streaks** and **irregular streaks**, or **regular vascular structures** and **irregular vascular structures**. As such, we expect the cosine similarities between the CAVs to confirm that these concepts are negatively correlated (or less similar to each other than to other concepts).

Spatial Dependence Some of the concepts have expected spatial dependencies, for example, **dark borders** and **dark corners**. Spatial norms could be used to confirm these spatial dependencies exist. Equally, for concepts such as the presence of a **ruler**, the spatial norms could confirm the CAVs have no overall spatial dependence.

17.1 Experiment Setup

As the dataset used by Yan *et al.* [42] is not publicly available, we reproduce their results using a similar publicly available dataset.

Model We finetune a ResNet50 on the ISIC 2019 dataset [8, 10, 39] for the binary classification of melanoma. We use a binary cross entropy loss and the Adam optimiser [24], training until convergence of validation loss to achieve an area under the receiver operating characteristic curve (AUC) of 0.91 on the validation split.

CAVs For the CAVs, as in Yan *et al.* [42], we use the derm7pt dataset [22]. There are 12 clinical concepts which have been expertly labelled within the dataset. We hand labelled three additional concepts, which were used in [42], of **dark corners**, **dark borders** and **ruler** which are possible confounders for the model. We defined **dark corners** as any image with a circular aperture which left the corners of the image black, **dark borders** as any image containing rectangles of blacked out areas and **ruler** as any image containing a ruler. For each of the medical concepts, there are three labels: typical/regular, atypical/irregular, and absent. When training CAVs for these concepts, we used images with the label of ‘absent’ as the negative probe dataset. This was done because using random images as the negative set gave low-quality CAVs, with accuracies of 50-65%. It is unclear from [42] what they used for negative sets. For training the CAVs we used 70 images per concept and used 30 different random seeds for the random negative probe set to get 30 CAVs per concept. Yan *et al.* [42] do not use TCAV, so this setup is different from the original paper.

17.2 Results

We first show that we can produce concept-based explanations for melanoma classification as in [42]. We then show how the use of our analysis tools impact the conclusions that can be drawn.

In Fig. 35, we obtain a high accuracy for the CAVs trained on confounders between 80-90%, but only 60-75% for the medical concepts. We hypothesise that this is due to the simplicity of the confounding concepts. This is supported by the accuracy reported in [42] where they also obtained a lower CAV accuracy for the medical concepts. The accuracy for the confounding concepts of **dark borders** and **dark corners** drops in later layers. This is likely due to the spatial nature of the concepts – an idea further supported by Fig. 38 where the CAVs in later layers have reduced spatial distinction.

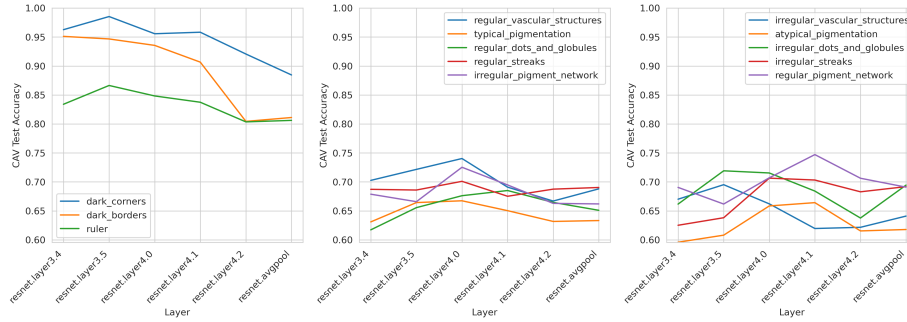


Fig. 35: Mean test accuracy for the linear classifiers from which the CAVs are generated for all concepts analysed on the melanoma datasets (split by concept type - confounders, regular, irregular)

Consistency – Consistent TCAV scores across layers indicate reliable explanations. The TCAV scores in Fig. 36 are consistent across layers, providing more confidence in using them to explain the model’s behaviour. In terms of understanding the model, the scores provide some evidence that it operates similar to human experts, as the TCAV scores for the atypical/irregular medical concepts are high for the malignant class, as expected, and the confounding concepts are often not significant, providing no evidence that the model is sensitive to the confounders.

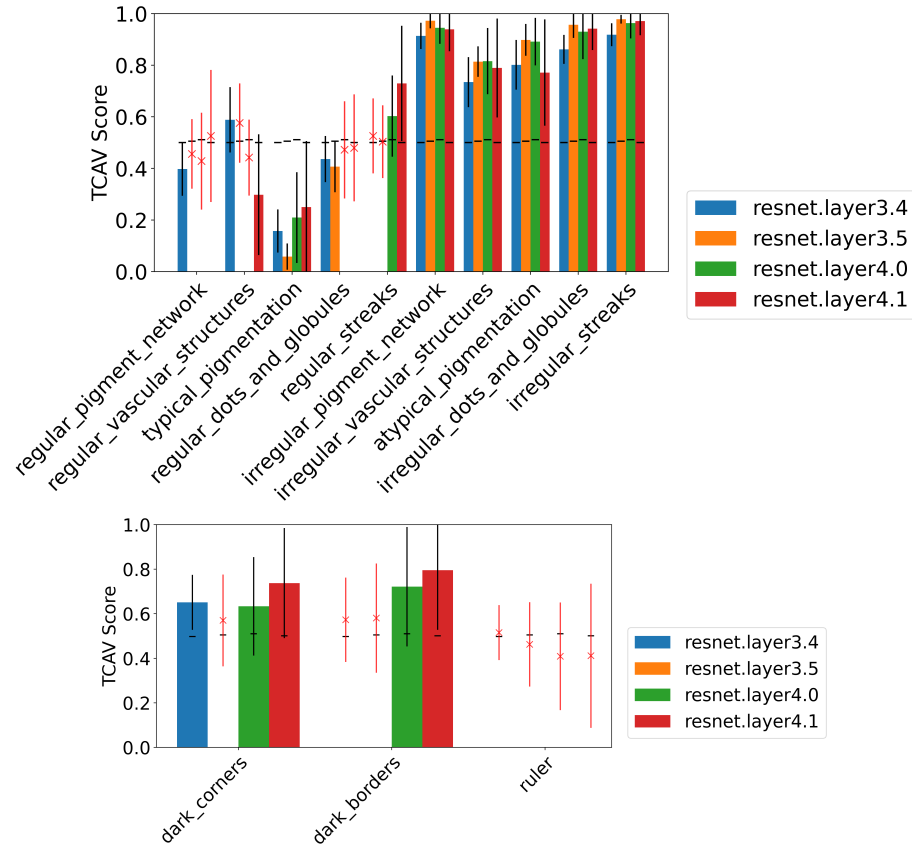


Fig. 36: TCAV scores for the melanoma use-case. Top: medical concepts, Bottom: potential confounders. The standard deviation is shown in black for significant results and red for insignificant results. The mean TCAV score for random CAVs are shown as horizontal black lines.

Entanglement – Unexpected similarities between concepts suggest further experiments need to be performed. Interestingly, in Fig. 37, the CAVs with opposed meanings often appear to be the most similar to each other. For example, `regular vascular structures` has a negative or zero similarity with all concepts except `irregular vascular structures` (with a similarity of 0.11). This could be due to our choice in negative set for the probe datasets as these two concepts share the same negative set. If we were to continue analysing these results, this hypothesis should be explored and alternative approaches attempted. Equally, we would require a domain expert to compare which concepts are most similar to each other to check whether the relative similarities of the concepts make sense.

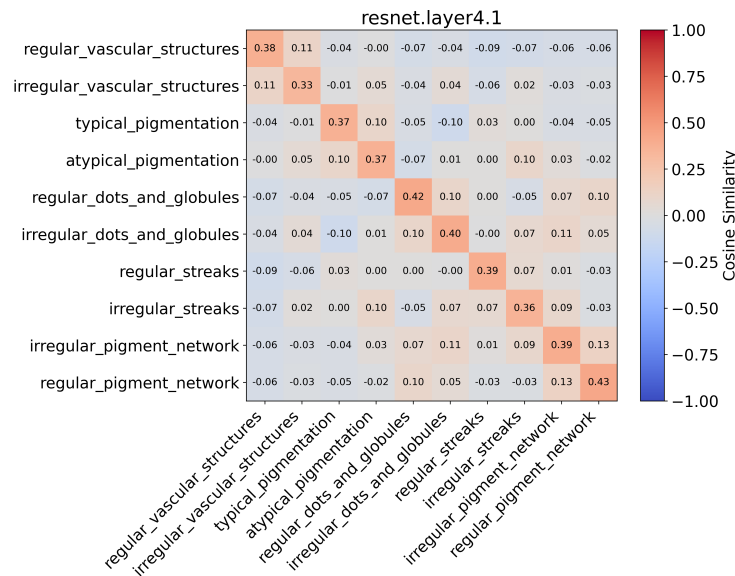


Fig. 37: Mean pairwise cosine similarities between 30 CAVs for different concepts from the melanoma use-case.

Spatial Dependence – The spatially dependent confounders are better represented in earlier layers. The spatial norms and means in Figures 38 and 39 show a clear spatial dependence in the center for each of the medical concepts across all layers. This aligns with expectations, as the dataset requires the skin lesion to be centered in the image and each concept is related to the appearance of the lesion. The **dark corners** and **dark borders** concepts, however, show deviations to this pattern in the earlier layers, with **dark corners** having high spatial norms in the corners and **dark borders** high spatial norms in the top. This is desirable, as these confounding concepts depend on features at the edge of the image, away from the lesion. Along with the accuracies in Fig. 35, this suggests that the CAVs in earlier layers better represent these spatially dependent concepts. For **dark borders**, we may want to examine the probe dataset and collect more images with dark borders in locations other than the top, as the CAV seems focused on the top of the feature space – this is even more apparent in the spatial means of Fig. 39.

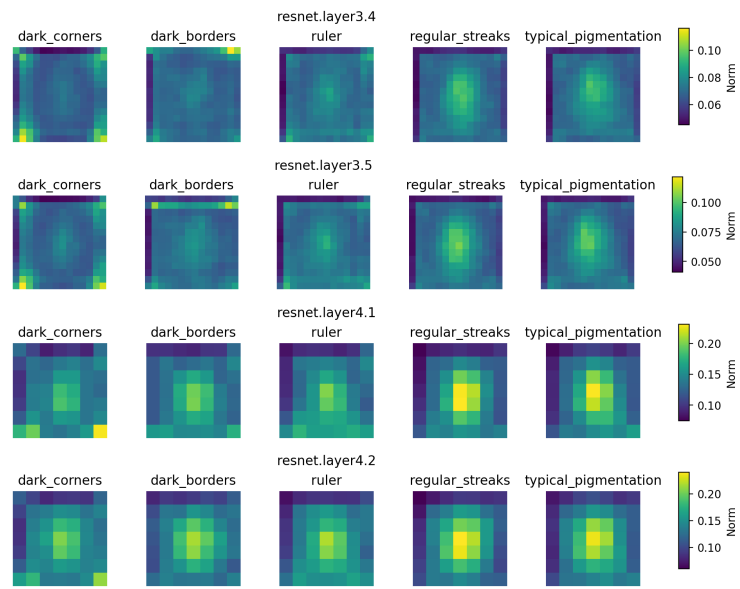


Fig. 38: Mean CAV spatial norms across 30 CAVs for a selection of concepts and layers in the melanoma use-case.

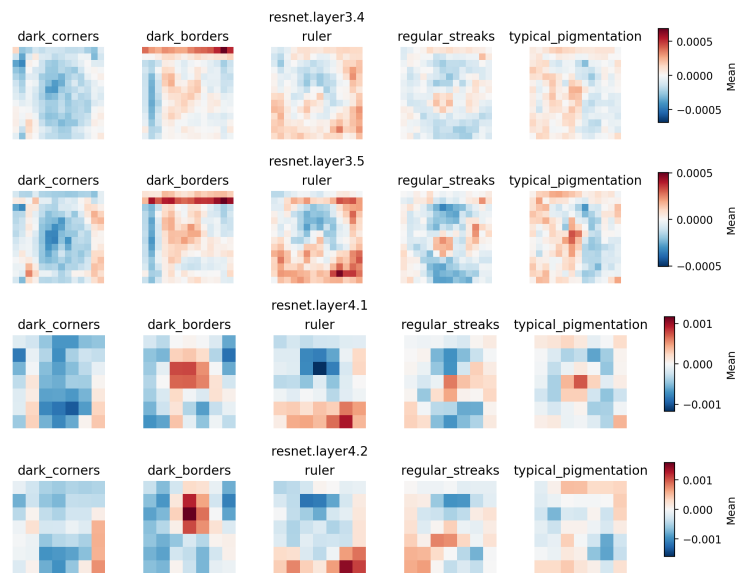


Fig. 39: Mean CAV spatial means across 30 CAVs for a selection of concepts and layers in the melanoma use-case.